Implications of the Varying Permeability Model for Reverse Dive Profiles

David E. Yount
Department of Physics and Astronomy
University of Hawaii
Honolulu, Hawaii 96822

Eric B. Maiken
EMAI
561 Keystone Ave.
Reno, Nevada 89503

Erik C. Baker
Comprehensive Design Architects/Engineers
3054 Enterprise Drive
State College, Pennsylvania 16801

Accepted for publication by: The American Academy of Underwater Sciences (2000)

Presented at the
Reverse Dive Profiles Workshop
October 29 and 30, 1999
Smithsonian Institution, Washington, D.C.

Abstract

There is currently considerable interest in using physics-based bubble models to compute decompression schedules. At the center of this activity is the Varying Permeability Model (VPM), in which as few as three nucleation parameters and one decompression parameter replace traditional M-values as the ascent limiting criteria. For deep and intermediate portions of decompression profiles, supersaturation limits calculated by the VPM are less than those of conventional dissolved-gas algorithms. Progress in the application of this model has been aided by the voluntary Internet information-exchange group known as the "Decompression List."

Introduction

The Varying Permeability Model (VPM) (Yount 1979a) fundamentally incorporates diving depth into the formulation of ascent criteria. For square-profile dives, where the crushing pressure p_{crush} is equal to the diving depth, the minimum VPM supersaturation gradients have been experimentally determined to be proportional to p_{crush}. With the definitions that a *reverse dive* is a *deeper-than-previous dive,* and a *forward dive* is a *shallower-than-previous dive*, a clear distinction can be made that forward diving places the largest p_{crush} first in series of exposures. This applies to the time-scales of both repetitive and single dives. In the case of non-square profiles, such as very slow descents followed by direct ascents, the determination of p_{crush} is subtle, and relates to the maximum difference attained between dissolved gas tension and the ambient pressure of the dives. Moreover, the VPM predicts that the maximum benefit from crushing gas nuclei is achieved by doing the deepest part of a prolonged or repetitive exposure first.

Here, a dive is considered repetitive when the surface interval between it and its predecessor is sufficiently short that the first dive *influences* the second. Examples of such an influence, as compared to a single isolated dive, are an increased incidence rate for decompression sickness (DCS), enhanced Doppler bubble counts, and the exacerbation of various precursors of decompression sickness, such as fatigue, malaise, or discomfort. Possible mechanisms by which one dive might influence another include excess dissolved gas (gas loading), unresolved free gas (gas bubbles), and changes in the underlying size distribution of bubble formation nuclei (gas nuclei). The first of these effects is accounted for in conventional dissolved-gas algorithms, which keep track of inert-gas loads. The second and third can be addressed in the context of the VPM, which is the focus of this work.

This paper is organized into three sections, beginning with consideration of how the field experience of divers is being used to modify commonly available neo-Haldane tables by incorporating deep decompression stops into ascents. We then review the Varying Permeability Model's foundation in bubble formation experiments, and experimental implications for reverse diving profiles. The final section discusses use of the VPM to formulate diving tables, and applies the model to the analysis of forward and reverse diving profiles.

I. The Influence Of Technical Diving On Decompression Practice

Over the past decade, decompression diving has entered the mainstream of upper-end sport diving. The intrinsic risks associated with decompression are widely known, and more than a century has been spent in trying to overcome them. Given these facts, it is surprising that so many highly-intelligent and highly-educated people have recently put aside conventional tables designed and tested by competent professionals, and elected to design and test their own. Recalling Abraham Lincoln’s famous aphorism about lawyers,

one is tempted to ask, “Doesn’t the diver who designs his own tables have a fool for a client?”

The first reason why some technical divers prefer to design and test their own tables is that they can. Many have computational abilities that far exceed those of decompression pioneers, who produced operational tables in an era when the physics of bubble formation in aqueous media was poorly understood, and commercial decompression programs, dive computers, personal computers, and powerful software did not exist. The second reason technical divers might choose to design their own tables is that they have easy access to unconventional algorithms, such as the Thermodynamic Model (Hills 1966), the Varying Permeability Model (Yount and Hoffman 1986), and the Reduced Gradient Bubble Model (Wienke 1991). By “easy access” we mean that they have both the mathematical skills needed to understand these published algorithms and the computational skills needed to implement them, if need be, from scratch. The third reason is that many technical divers are dissatisfied with the results of conventional algorithms. There is also widespread suspicion that something is missing, that there is a need for “deep stops” as called for by LeMessurier and Hills (1965), by Yount and Strauss (1976), by Hennessy and Hempleman (1977), and by others. The VPM tables calculated by Yount and Hoffman (1986) also call for deep stops, but because those tables were calibrated using US Navy (1977) and Royal Navy Physiological Laboratory (1968) tables, which are now considered aggressive and obsolete, the original VPM tables are also considered too aggressive.

One of the pioneers in this endeavor was marine biologist Richard Pyle, who serendipitously discovered the benefit of deep stops while collecting ichthyologic specimens (Pyle 1996).

> “…so it’s abundantly clear… my empirically-derived deep-stop method has more to do with the physiology of fish than … Humans. …I first noticed the apparent benefit on dives when I had to stop deep to vent gas from fish’s swim bladders. Because of that observation, I repeated those stops on dives when I didn’t collect fish….”

Pyle simply felt better after completion of dives that incorporated deep stops. So what we have here is a new paradigm in which a technical diver modifies an existing table, tries it out on himself, and decides to keep or reject the modification to his diving practice on the basis of how he “feels.” While more subjective than the usual method of “titrating” Navy divers five at a time, this empirical, try-it-out-on-yourself method is actually far more sensitive because it replaces the bimodal endpoint of bends/no-bends with a continuous scale that associates greater comfort with greater safety. It is important to note that these divers often have personal experience with a full range of dcs symptoms, and are therefore discerning observers. There is another reason why Pyle’s method is safer: He is moving away from the bimodal endpoint where some divers get bent, rather than toward it. In seeking greater safety, Pyle definitely has an astute client!

Although it is difficult to quantify testimonials of this sort, they *are* very compelling. Given enough of them, one feels intuitively that they must have some validity. Why is this so? Imagine that a scientist is studying a group of athletes who are required to complete some arduous task, such as a decathlon. The usual method of titrating divers would be equivalent to recording only the number of athletes who competed and the number who got hurt. World record times and distances would be of no interest, nor would the scientist doing such a "titration" care how hard the athletes trained, how tired they got, how sore their muscles were, how much they ate, or how long they slept. A good sports writer, on the other hand, would probably gloss over the casualty report and focus on interviews and anecdotes. In this way, he would reveal what it felt like to compete in the decathlon and help readers like us to experience--along with the athletes--the thrill of victory and the agony of defeat. Indeed, the things that would interest sports fans the most are the very things that the narrowly focused scientist would miss. With this analogy in mind, we have solicited testimonials relevant to reverse dive profiles, deep stops, VPM, and gradient factors from the Decompression List. A link to the Deco List web page for the Reverse Dive Profiles Workshop can be found on-line at: `http://www.phys.hawaii.edu/~dey`.

II. The Varying Permeability Model

Numerous experiments demonstrate that cavitation thresholds can be significantly raised by degassing or by briefly exposing the sample to high pressure (Harvey et al. 1944, Yount and Strauss 1976, Gerth and Hemmingsen 1976). These are specific tests for stable gas nuclei, yet the very existence of such entities is surprising. Gas phases larger than 1 μm in radius should float to the surface of a standing liquid, while smaller ones should dissolve rapidly due to the surface tension γ. Earlier proposals for coping with this dilemma were critically reviewed by Yount et al. (1977), and the Varying Permeability Model was introduced as an alternative to address the inconsistencies between experimental results and existing models (Yount et al. 1977, Yount 1979a).

Over the years, the evidence that stable microbubbles actually exist in aqueous media has become very compelling. Medwin (1974) has inferred the presence of large and persistent populations in seawater from acoustic measurements, and Johnson and Cooke have photographed their formation and stabilization in this liquid (1974). Candidates have also been observed in gelatin and distilled water using both light and electron microscopes (Yount, Gillary, and Hoffman 1984), and several of their physical properties, such as their size distribution and skin thickness, were measured and found to be consistent with VPM expectations.

II.1 VPM Nuclei

The Varying Permeability Model postulates that cavitation nuclei consist of spherical microbubbles that are small enough to remain in solution and strong enough to resist collapse. The mechanical compression strength is provided by an elastic skin or

membrane composed of surface-active molecules. Ordinarily, VPM skins are permeable to gas, but they can become effectively impermeable when subjected to large compressions, typically exceeding 8 atm (0.8 MPa).

By tracking changes in nuclear radius caused by increases or decreases in ambient pressure, the VPM has provided precise quantitative descriptions of several bubble-counting experiments carried out in supersaturated gelatin (Yount and Strauss 1976, Yount and Yeung 1981, Yount, Yeung, and Ingle, 1979). The model has also been used to trace levels of incidence for decompression sickness in a variety of animal species, including salmon, rats, and humans (Yount 1979b, Yount 1981), and to calculate diving tables for humans (Yount and Hoffman 1983, 1986, 1989). The rate at which individual VPM nuclei evolve from one equilibrium state to another has been investigated theoretically, and a statistical process by which the equilibrium size distribution of an entire population of VPM nuclei may be generated or regenerated has been proposed (Yount 1982). In the most recent paper in this series (Yount 1997), the third independent derivation of VPM was obtained by applying thermodynamic methods formulated by Kozlov and Markin (1990) to describe the strongly-curved amphiphilic interfaces found in micelles, emulsions, giant bilayer vesicles, and biological membranes. The VPM nucleus is thus another example of such a system.

Some additional features of the Varying Permeability Model are depicted in Fig. 1 (Yount 1982). In Fig. 1(a), the internal gas pressure is p_{in}, and the ambient hydraulic pressure is p_{amb}. If there were no skin, the situation would be described by the well-known Laplace equation,

$$p_{in} = p_{amb} + \frac{2g}{r} \quad (gas\ bubbles), \tag{1}$$

which suggests that p_{in} is always larger than p_{amb} in the case of ordinary gas bubbles.

VPM nuclei differ from ordinary gas bubbles because the surface-active molecules in the skin generate a skin compression Γ and a skin pressure $2\Gamma/r$ that oppose the surface tension γ and surface pressure $2\gamma/r$ of the surrounding water. Together, they yield a new expression for mechanical equilibrium,

$$p_{in} + \frac{2\Gamma}{r} = p_{amb} + \frac{2g}{r} \quad (gas\ nuclei). \tag{2}$$

Because Γ can be larger than γ in a spherical environment, the net surface tension $\gamma' = \gamma - \Gamma$, and the net surface pressure, $p_{in} - p_{amb} = 2(\gamma - \Gamma)/r$, can assume negative as well as positive values. In this case, mechanical equilibrium can be achieved regardless of whether p_{in} is larger or smaller than p_{amb}.

II.2 Bubble Formation Experiments

Excess surfactant molecules are stored in a reservoir, which is represented in Figs. 1(b) and Fig. 1(c) as a concentric shell of negligible thickness that lies just outside the skin and thus has the same radius *r*. Surfactant molecules move from the skin to the reservoir when the radius decreases, and they move from the reservoir to the skin when the radius increases. In this way, the "crumbling compression" γ_c, which is the maximum possible value of the skin compression Γ, is preserved.

Fig. 1(d) shows a rudimentary pressure schedule used to study bubble formation in supersaturated gelatin. The schedule consists of a rapid compression from p_o to the maximum pressure p_m, saturation of the sample at $p_s = p_m$, and a rapid decompression from p_s to the final pressure p_f. The term "rapid" means operationally that the process involves no change in the dissolved gas tension τ. Saturation at $p_s = p_m$ means that τ assumes the value p_s prior to decompression. The maximum over-pressure or crushing pressure is then

$$p_{crush} \equiv (p_{amb} - t)_{\max} \tag{3a}$$

$$= (p_m - p_0), \tag{3b}$$

and the maximum supersaturation is

$$p_{ss} \equiv (t - p_{amb})_{\max} \tag{4a}$$

$$= (p_s - p_f). \tag{4b}$$

A salient feature of bubble formation in supersaturated gelatin (Yount and Strauss 1976) is that the bubble counts depend only on p_{crush} and p_{ss}, and not on the Haldane ratio, p_s/p_f. Two schedules having the same values of p_{crush} (300 psig) and p_{ss} (150 psig) are shown, respectively, in Figs. 2(a) and 2(b). The first has a Haldane ratio of 11.2, and the second has a Haldane ratio of 1.91, yet the average yields, around 16 bubbles per gelatin sample, were nearly the same. The schedule shown in Fig. 2(c) has the same p_{ss} (150 psig) and Haldane ratio (11.2) as that shown in Fig. 2(a), but the average yield was 30 times higher, around 500 bubbles per sample, because p_{crush} (150 psig) was only half as large.

Yount and Strauss (1976) also learned how to decompress gelatin safely. Their prescription, illustrated in Fig. 2(d), calls for "deep stops" and a constant off-gassing gradient, $\tau - p_{amb} = p_{ss}$, throughout the ascent. The theoretically optimum decompression required 12 min and yielded an average of 0.42 bubbles per sample. The corresponding US Navy schedule required 17 min and yielded an average of 12.9 bubbles per sample.

Because p_f is ordinarily greater than or equal to p_o, p_{ss} is ordinarily less than or equal to p_{crush}:

$$p_{ss} \le p_{crush}. \tag{5a}$$

To explore the region defined by

$$p_{ss} > p_{crush}, \qquad (5b)$$

Yount and Yeung (1981) used slow compressions or stepped compressions, which permitted a significant rise in the dissolved gas tension ô while the ambient pressure p_{amb} was increasing. For the pressure schedule shown in Fig. 3, the maximum over-pressure, $p_{crush} = (p_{amb} - \tau)_{max}$, occurred on the very first step, and was simply the magnitude of the initial compression, 4.1 atm. Any other increments, whether they preceded or followed the largest, had no effect. The maximum supersaturation was p_{ss} = 20.4 atm, which was about five times larger than p_{crush} = 4.1 atm.

Fig. 4 is a graph of p_{ss} versus p_{crush} for constant bubble number *N*. The "old region" is defined by Eq. 5(a) and the "new region" by Eq. 5(b). As expected, all of the data points in the old region and many of those in the new lie on a family of straight lines generated by the Varying Permeability Model. The smallest initial nuclear radius r_o probed in this experiment was approximately 0.0l μm. At these small radii, the classical VPM begins to break down because the thickness of the surfactant skin was not taken into account. When this deficiency was corrected, reasonable fits to all of the data in the old region were obtained (Yount and Yeung 1981).

Fig. 3 can be regarded as a reverse dive profile in the generic sense that the latter part of the exposure is deeper than the former. The yield in the original or "reverse" direction was greater than 200 bubbles per sample. The yield in the opposite or "forward" direction, corresponding to p_{crush} = 20.4 atm and p_{ss} = 6 atm, would average less than 0.1 bubble per sample, as can be inferred from Fig. 4. The lesson to be learned from these data is that it's best to crush gas nuclei by doing the deepest part of a prolonged exposure first.

II.3 The VPM and Reverse Profile Diving

Yount and Hoffman applied the VPM to formulate diving tables for non-repetitive dives, (Yount and Hoffman 1986). Wienke's *Reduced Gradient Bubble Model* (RGBM) (Wienke 1991) extended the VPM to repetitive-diving situations, such as reverse-profile diving. What does the VPM have to say about reverse-profile diving? We shall draw some conclusions directly from the VPM and certain key experiments, which, together with the following assumptions, summarize our current application of the VPM to the etiology of decompression sickness.

II.3.1 A Set of Assumptions

i) The VPM is applicable to decompression sickness in humans.

ii) Gelatin bubble-counting experiments are applicable to in-vivo DCS.

Assumptions *i* and *ii* are consistent because the VPM was formulated to describe the gelatin experiments. However, both are needed because the VPM might be applicable even if the gelatin experiments are not, and vice versa.

iii) Abnormalities that exist at the start of a dive have greatest impact for stressful dives.

Because the second dive in a reverse-dive profile is the more stressful, any abnormalities or irregularities produced by the first dive would have greater impact in the reverse-dive situation than in the forward situation. Saying this another way, if two successive dives are planned, it's best to do the more stressful dive first while the condition of the diver is still pristine.

iv) The number of bubbles present after a typical first dive is large.

Indeed, the number is probably much larger than the number of super-critical nuclei because the growth of a primary bubble in tissue is limited by the local tissue deformation pressure, which pumps most of the gas liberated at the primary site into neighboring secondary sites. Instead of producing one large bubble, therefore, a super-critical nucleus usually produces many small ones, a primary, and many secondaries. Gaspare Albano (1970) published a series of photomicrographs demonstrating that one primary bubble can produce a "rosary" of secondary bubbles. Cowley, Allegra, and Lambertsen (1979) observed the time course of secondary-bubble production by subjecting the ears of New Zealand White rabbits to isobaric counterdiffusion at 1 atm and recording the pressure drops that occurred inside a primary bubble whenever the tissue cleaved. A more detailed discussion of the rosary phenomenon and secondary-bubble production can be found in the paper given by Yount (1979c) at the Workshop on Isobaric Inert Gas Counterdiffusion.

II.3.2 Persistent Bubbles and Reverse Dive Profiles

From the point of view of the VPM, any gross bubbles left over from the first dive would be expected to stabilize because the surrounding blood or tissue is loaded with surfactants. Like old soldiers, old bubbles *in vivo* never die, they just become large stable gas nuclei. According to the "ordering hypothesis" (Yount et al. 1977, Yount 1979a), if there are more large nuclei present at the beginning of the second dive, there will be more large nuclei present at the end. If there are more large nuclei present at the end of the second dive, more primary bubbles will form, and the volume of released gas will be larger than expected had the second dive been performed as a single isolated dive. While it has been demonstrated mathematically that VPM nuclei of any initial size will eventually replicate the primordial or pristine size distribution (Yount 1982), the surface interval between two dives that are spaced closely enough to be deemed repetitive, whether forward or reverse, would be too short for full restoration to occur. It should also be noted that full restoration in the mathematical sense implies full restoration of the radial dependence with no loss of nuclei and hence no change in the total number N_o.

This mechanism has important implications for reverse dive profiles. It does not arise in conventional algorithms that only keep track of inert-gas loads. Though important and unique, the mechanism is difficult to quantify because the number and size-distribution of any microbubbles that may be present at the beginning of the second dive are unknown. Nor is it certain that the VPM is immediately applicable to stable microbubbles with radii as large as, say, 10 to 100 μm: Although such populations are known to exist in nature and have actually been observed in sea water (Medwin 1974), the surface pressure $2\gamma/r$ is less than the tissue-deformation pressure in this size range (Cowley, Allegra, and Lambertsen 1979), and both would have to be taken into account. Even if the VPM is applicable in some modified way, the parameter values for stable microbubbles recently formed from gross bubbles could differ from those needed to describe primordial nuclei that have "aged" for days or weeks.

A second mechanism through which the existence of microbubble nuclei can influence an ensuing exposure in a reverse-dive sequence is by changing the underlying size distribution *N(r)*. This effect can go either way. If a deep first dive "crushes" gas nuclei, rendering them smaller, the second dive will be safer than usual, assuming that appropriate allowance has been made for any excess dissolved gas that remains in the various tissues or compartments. If, on the other hand, the quantity of residual dissolved gas is large, it can reduce the effective crushing pressure for the second dive. Less crushing implies that there will be more large nuclei, more primary bubbles, more secondary bubbles, and more free gas than would have been present had the second dive been performed as a single, isolated excursion.

III. The Vpm in Practice

The confluence of a number of technologies, including the advent of the Internet, and widespread sport decompression and mixed-gas diving, have lead to world-wide interest in decompression schedules that emphasize small supersaturations. This section discusses the use of the VPM to calculate diving tables and applies the methods to the analysis of an example set of reverse diving profiles.

III.1 VPM-based Decompression

A derivation of the VPM equations, based on consideration of compression of an elastic shell, leads to the relationship between differential changes in nuclear radius ∂r, external pressure ∂p_{amb}, and internal pressure ∂p_{in}

$$2(g_c - g)\frac{\partial r}{r^2} = \partial p_{in} - \partial p_{amb}, \qquad (6)$$

where Γ of Eq. (2) has been replaced with the crumbling compression γ_c (Yount 1979a). Extending previous applications of Eq. (6), which set $\partial p_{in} = 0$ in the permeable regime,

we explicitly consider the effects of compression and decompression rate by setting the internal pressure p_{in} equal to the dissolved gas tension τ.

Section III.4.1 applies a numerical method to compute solutions to Eq. (6) for dives with non-instantaneous descent and ascent rates. An analytical solution of Eq. (6) results from integration over compression and decompression cycles, and use of the Laplace equation as an ascent-limiting criteria. The resulting minimum allowed supersaturation gradients for a set of *j* parallel compartments are expressed as

$$P_{ss\ j}^{\min} = \frac{2g\,(g_C - g)}{g_C\, r_{0\,j}} + \frac{g}{g_C}\Delta_j\,. \tag{7}$$

Here, our notation generalizes the notation used by Yount (1979a) by calculating the minimum gradients for a set of compartments with time-dependant tensions τ_j , and a set of initial nuclear radii distributed across compartments as r_{0j}. For an instantaneous descent and ascent, $\Delta_j \rightarrow (\ p_m - p_0\ )$, $r_{0\,j} \rightarrow r_0$, and Eq. (7) reduces to the Yount (1979a) form, with a single $P_{ss}^{\min}$ for all compartments. In the case of a gradual descent, Δ_j is a set of effective crushing pressures $p_{crush\ j}$ that follow from application of Eq. (3a) to a set of compartments with time-dependent dissolved gas tensions τ_j. As discussed in sections I.2 and III.3, these pressures are less than the full crush attained for an instantaneous descent, with the fastest half-time compartments affected the most. Use of the method of Schreiner and Kelley (1971) to compute compartment tensions τ_j during a descent at a crushing rate r_C, over a crushing time t_C yields

$$\Delta_j = (p_m - p_0)(1 - f_{N2}) + \frac{f_{N2}\, r_C}{k_j}(1 - \exp(-k_j\, t_C)), \tag{8}$$

with $\ln(2)/k_j$ corresponding to the *j*'th compartment's half-time. In the limit of a fast descent, $t_C \rightarrow 0$, the crushing pressure is $r_C\ t_C\ = (\ p_m - p_0\ )$, and Eq. (8) reduces to the Yount (1979a) form.

The Yount and Hoffman (1986) method for calculating VPM-based diving tables follows from the dynamic critical volume hypothesis, which restricts the volume of free gas evolved in each compartment *j* by the condition

$$\int_0^t (N_{actual} - N_{safe})\ P_{ss\ j}^{new}(t')\,dt' \quad \le a V_{critical}\,. \tag{9}$$

The excess bubble population is $(N_{actual} - N_{safe})$, a is a proportionality constant, and $V_{critical}$ the critical volume, as discussed by Yount and Hoffman (1986). For diving profiles with direct ascents and descents in the permeable regime, Eq. (9) can be solved analytically. With an assumed *linear* ascent rate, the allowed supersaturations for the *j* compartments are

$$P_{ss}^{new}{}_{j} = \tfrac{1}{2}[b_j + \sqrt{b_j^{\,2} - 4c_j}] \qquad (10a)$$

with

$$b_j = P_{ss}^{\min}{}_{j} + \frac{g}{g_C}\frac{l}{t_D + k_j^{-1}} - \frac{(t_j^{dive} - p_m)t_D}{2(t_D + k_j^{-1})} \qquad (10b)$$

$$c_j = \frac{g^2}{g_C^2}\frac{l(p_m - p_0)}{t_D + k_j^{-1}} - \frac{P_{ss\,j}^{\min}(t_j^{dive} - p_m)t_D}{2(t_D + k_j^{-1})}. \qquad (10c)$$

The total ascent time t_D is always greater than zero for the linear ascent rate. l is proportional to the critical volume, and τ_j^{dive} denotes the set of compartment tensions at the end of the dive.

The last terms in the expressions for b_j and c_j add to the original expressions for b and c derived by Yount and Hoffman (1986), and reduce to the original forms for saturated, non-metabolizing systems with $\tau_j^{dive} \rightarrow \tau \approx p_m$. These new terms can have magnitudes that are comparable to the others, and increase the gradients allowed during ascents from the Yount and Hoffman values for equivalent ascent times and pressurization-depressurization schedules. The Yount and Hoffman (1986) VPM decompression algorithm uses an iterative method to solve the set of Eqs. (7) and (10), starting with calculation of the minimum allowed supersaturation gradients $P_{ss\,j}^{\min}$, and then successively updating the calculation until t_D converges. This results in the relaxation of the stringent $P_{ss\,j}^{\min}$ gradients into the set of new, more liberal gradients $P_{ss\,j}^{new}$.

III.2 Open Source-Code VPM-Based Decompression Program

The Yount and Hoffman (1986) VPM algorithm was implemented in a series of open source-code *BASIC* language computer programs, which have been freely available to programmers since the *tek95* diving technology conference (Maiken 1995). These programs expand on the original algorithm by modeling generalized nitrox decompression dives with multiple stages, gas switches, and constant ppO_2 rebreather diving. As of October, 1999, the programs have been distributed to approximately 150 diving programmers worldwide, and the VPM methods have been integrated into a number of publicly available programs.

III.3 Hydrostatic Pressure, Dissolved Gas, and the VPM Gradients

A diver's exposure to hydrostatic pressure affects ascent criteria through the dependence of Eqs. (7) and (10) on the crushing pressure, and inert gas tensions τ_j^{dive}. As an example of the roles of hydrostatic pressure in setting VPM supersaturation gradients, consider nitrox diving. Conventional nitrox use emphasizes the reduced inert-gas loading of nitrox compared to air for identical profiles. Nitrox decompression calculations are

often based on the equivalent air depth (EAD), where the EAD is less than the dive depth. The VPM considers the compartment tensions resulting from a nitrox profile and an air dive to the EAD to be virtually identical. However, for a given nuclear distribution, the VPM gradients are determined by p_{crush}. Except for the fastest compartments, this results in a set of larger, more liberal gradients compared to a set calculated for the EAD. Although the dissolved gas EAD concept yields conservative ascent gradients, it does not completely determine ascent criteria in the VPM.

For repetitive nitrox diving, the actual dive depths should be used as criteria to determine whether a set of profiles is forward or reverse. For example, if two dives are made to a depth of 100 feet, separated by a surface interval on air, with one on 36% nitrox and the other on air, the nitrox dive would conventionally be treated as an air dive to the equivalent air depth (EAD) of 75 feet for application of diving tables. Nonetheless, these would not be considered reverse profiles in the VPM.

Yount and Yeung (1981) demonstrated that a slow descent inhibits the crushing of nuclei, and thus leads to enhanced bubble growth compared to rapid compressions. For a linear descent, this effect is quantified by Eqs. (7) and (8), which predict that the allowable minimum supersaturations $P_{ss\,j}^{\min}$ of fast half-time compartments are reduced compared to the slower half-times. Although this effect inverts the conventional ordering of M-values by compartments, it is physically reasonable. This is because exposure of nuclei in fast compartments to large dissolved gas tensions during descent results in diffusive growth, and larger equilibrium radii compared to nuclei in slow compartments. Nonetheless, for typical sport diving profiles, Eqs. (10) invert the minimum gradients calculated by Eq. (7), and the $P_{ss\,j}^{new}$ are ordered with the supersaturations of the slow compartments less than those of the fast compartments. For non-standard, though perhaps operationally common profiles, the $P_{ss\,j}^{\min}$ may control the ascent. One example is a saw-tooth exposure with a very gradual descent to a final, maximum depth, followed by a direct ascent. In this case, the VPM distinctly recommends reduction in the allowed supersaturation gradients compared to a dive made with a punctual descent to the same maximum depth.

III.4 Reverse Diving Profile Workshop Series of Exposures

The organizers of the *Reverse Dive Profiles Workshop* asked participants to specifically consider the series of forward and reverse diving profiles summarized in Table I. Recognizing that these profiles fall within the context of sport diving, and for purposes of our graphical analysis, we use the contemporary set of Bühlmann ZH-86 air diving tables as a baseline reference in Table II. The profiles generated by Bühlmann's tables are similar to those produced by the range of dive computers in current use by sport divers.

Table I. Reverse and Forward Dives

Reverse Dive Series (A)			
Series	First Dive Profile	Surface Interval	Repetitive Dive Profile
1A	40 fsw to NDL	30 min	100 fsw
2A	40 fsw to NDL	60 min	100 fsw
3A	40 fsw to NDL	120 min	100 fsw
Forward Dive Series (B)			
Series	First Dive Profile	Surface Interval	Repetitive Dive Profile
1B	100 fsw to NDL	30 min	40 fsw
2B	100 fsw to NDL	60 min	40 fsw
3B	100 fsw to NDL	120 min	40 fsw
(NDL: no-decompression limit)			

III.4.1 A Numerical Calculation of a Dynamic Minimum Supersaturation

We have implemented a numerical solution to Eq. (6), which tracks the radii and minimum allowable gradients $P_{ss\,j}^{\min}$ for each compartment during decompression from dives in the permeable regime. The nitrogen partial pressures τ_j were computed by the method of Schreiner and Kelley (1971), using their alveolar ventilation equation. The alveolar partial pressure of inert gas was based on the nitrogen fraction f_{N2} of the breathing mixture, standard values for $P_A\,CO_2$ and $P_A\,H_2O$, and a respiratory quotient of 0.9. The set of 16 nitrogen compartments of the Bühlmann ZH-L16 Calculation Model (Bühlmann 1995) were used to parameterize the spectrum of tissue half-times in the human body, with half-times ranging from 5 to 635 min.

Under this framework, the internal pressure p_{in} of gas nuclei is equal to the dissolved inert gas tension τ_j of the surrounding compartment. The analysis program tracks an array of radii across the 16 compartments. At the beginning of the first dive, the radius in each compartment is assigned a specific value, r_0. As the dive progresses, the program updates the radius for each compartment based on the instantaneous crushing or supersaturation pressures.

Table II. Profiles Based On Bühlmann ZH-86 Air Decompression Tables

Reverse Dive Series (A)

Series	First Dive	NDL	RG	SI	RG	RNT	Repetitive Dive
1A	40 fsw	125 min	G	30 min	F	30 min	100 fsw.[1]
2A	40 fsw	125 min	G	60 min	D	19 min	100 fsw.[2]
3A	40 fsw	125 min	G	120 min	B	11 min	100 fsw.[3]

[1]Because NDL = 17 min and RNT = 30 min, it is already a decompression dive. Modeled as a "spike" dive to 100 fsw, followed by immediate ascent. Deco stops at 20 fsw for 2 min and 10 fsw for 7 min.

[2]Because NDL = 17 min and RNT = 19 min, it is already a decompression dive. Modeled as a "spike" dive to 100 fsw, followed by immediate ascent. Deco stop at 10 fsw for 5 min.

[3]Because NDL = 17 min and RNT = 11 min, the NDL is reduced to 6 min.

Forward Dive Series (B)

Series	First Dive	NDL	RG	SI	RG	RNT	Repetitive Dive
1B	100 fsw	17 min	D	30 min	A	19 min	40 fsw.[4]
2B	100 fsw	17 min	D	60 min	A	19 min	40 fsw.[5]
3B	100 fsw	17 min	D	120 min	A	19 min	40 fsw.[6]

[4]Because NDL = 125 min and RNT = 19 min, the NDL is reduced to 106 min.

[5]Because NDL = 125 min and RNT = 19 min, the NDL is reduced to 106 min.

[6]Because NDL = 125 min and RNT = 19 min, the NDL is reduced to 106 min.

Abbreviations and Notes:
NDL = No-decompression limit (minutes), RG = Repetitive Group,
SI = Surface Interval (minutes), RNT = Residual Nitrogen Time (minutes),
fsw = feet of seawater (a unit of pressure).
Ascent rate is 30 fsw per minute.
A one-minute safety stop is required by the table for all no-decompression dives.

III.4.2 Graphical Analysis of Reverse Diving Profiles

We utilize pressure graphs to plot gas loadings, M-values, and VPM gradient lines against ambient pressure. The pressure graph is a useful tool for visualizing the salient characteristics of ascent or decompression profiles. An explanation and further examples of this method are given by Baker (1998a, 1998b). The Bühlmann ZH-L16B set of linear M-values for nitrogen are included to delineate the ascent limiting criteria of conventional dissolved-gas decompression algorithms.

In Figs. 5, 7, 9, 11, 13, 15, 17, and 19, the inert-gas loadings by compartment are compared with the respective Bühlmann ZH-L16B M-values. In Figs. 6, 8, 10, 12, 14, 16, 18, and 20, the inert-gas loadings by compartment are compared with the VPM isopleths of constant bubble number. These lines of fixed gradient are shown upon surfacing and are labeled with the initial radius r_0 assigned at the start of the dive series. A range of initial radii from 0.2 *m*m to 1.3 *m*m was selected on the basis of experimental values (Yount, Yeung, and Ingle 1979) and (Yount, Gillary, and Hoffman 1984).

The pressure graphs with the VPM criterion for bubble formation display two distinct lines for each of the twelve initial radii considered as can be seen in Fig. 20. These lines correspond to the envelope of Eq. (8) for the range of half-times modeled. The solid line labeled "Cpt 16" shows the gradient for bubble formation upon surfacing for Compartment 16, which has the slowest half-time for gas loading. Because of the very slow uptake of inert gas in this compartment, the effective crushing pressure during compressions will be very near the maximum possible (p_m - p_0), and the $P_{ss\,j}^{\min}$ are identical to the Yount (1979a) values. The dashed line labeled "Cpt 1b" shows the surfacing gradient for Compartment 1b, which has the fastest half-time for gas loading. Because of the fast uptake of inert gas in this compartment, the effective crushing pressure during compressions is reduced. As a result, the decrease in radius of gas nuclei will be less and the corresponding gradient for bubble formation will be smaller. The fixed gradient lines for bubble formation in Compartments 2 through15 (not shown) fall between the lines indicated for Compartments 1b and 16 on the pressure graphs.

In Fig. 5 the inert-gas loadings for a single 40 fsw dive do not exceed the respective M-values. Accordingly, this dive would be considered safe with regard to the conventional dissolved-gas algorithm. In Fig 6 the same gas loadings are compared with the VPM criterion for bubble formation, where it can be seen that the fastest compartments probe an initial radius r_0 of 0.6 *m*m. Based on the 0.8 *m*m value of Yount and Hoffman (1986), we would expect a substantial number of bubbles to form upon surfacing from this dive. This distinction is not revealed by the conventional dissolved-gas algorithm.

In Fig. 13 the inert-gas loadings for a single 100 fsw dive do not exceed the respective M-values. Accordingly, this dive would also be considered safe with regard to the conventional dissolved-gas algorithm. In Fig 14 the same gas loadings are compared with the VPM criterion for bubble formation, where it can be seen that the fastest compartments probe an initial radius r_0 of 0.3 *m*m. Based on the 0.8 *m*m value of Yount and Hoffman (1986), we would expect that the 100 fsw dive would produce far more bubbles upon surfacing than the 40 fsw dive. Again, this is a distinction not revealed by the conventional dissolved-gas algorithm.

The conventional algorithm fails to identify bubble formation and also fails to distinguish between the 40 fsw dive and the 100 fsw dive on the basis of their severity. The VPM, on the other hand, predicts that both dives will produce bubbles and that the

100 fsw dive would be more stressful than the 40 fsw dive. Given our assumption that any abnormalities existing at the start of a dive will have greatest impact for stressful dives, there is a clear indication that it would be best in this case to perform the 100 fsw dive first.

IV. Discussion

The Varying Permeability Model makes distinct recommendations for diving profiles. First, the crushing pressure p_{crush} should be maximized to the degree possible for any sequence of dives. This applies to single dives as well as to repetitive exposures. For punctual descents, p_{crush} is essentially equal to the change in hydrostatic pressure between the surface and the diving depth. For slow descents, Eq. (8) predicts a reduction in the allowable supersaturation gradients. Second, supersaturation gradients during dives should not exceed limiting values for bubble formation and/or volume of released gas. Following a conventional dissolved-gas algorithm, it is possible that a reverse dive profile, such a 40 fsw dive followed by a 100 fsw, can result in reduced values for effective p_{crush} as well as bubble-forming supersaturation gradients. Under this scenario, the total number of bubbles and the total volume of released gas can be substantial.

There is nothing inherently dangerous about a reverse dive profile providing that the decompression algorithm adequately takes into account excess dissolved gas (gas loading), unresolved free gas (gas bubbles), and changes in the underlying size distribution of bubble formation nuclei (gas nuclei). Only the first of these effects is accounted for in conventional dissolved gas algorithms. All three can be addressed within the context of the Varying Permeability Model.

Acknowledgements

The authors wish to thank the group of enterprising divers, programmers, and scientists that constitute the *decompression mailing list*. These individuals continue to constructively shape our views of decompression modeling and practice. We acknowledge Daniel Reinders, and Richard Pyle's helpful and spirited discussions. In particular, we are grateful for Rob Murray's initiative in creating and administering the Decompression Mailing List, which was instrumental in the writing of this paper.

Glossary Of Terms

Decompression List. The latest step in "open sourcing" decompression software is an electronic mailing list set up by Rob Murray in December 1998. In less than one year, the "Decompression List" has attracted more than 100 subscribers from all over the world, including prominent attendees at this workshop and all three authors of this paper. In a very real sense, the entire list is participating in the workshop because we have been discussing reverse dive profiles and related topics electronically for more than two months, and we expect to continue the dialogue after the workshop ends.

Deep stops. Technical divers commonly add deep stops to conventional ascent schedules. We shall define a *deep stop* as *any decompression stop that is deeper than the first stop computed using a conventional dissolved-gas algorithm*.

Open source-code. A non-compiled text listing of the commands used to write a computer program. The open source-code VPM program allows programmers to see the inner workings of the *BASIC* language computer program that implements the VPM-based decompression model. This program was the first open source-code decompression program available on the Internet.

Sport diving, by definition, *involves the use of only one nitrogen-oxygen breathing gas throughout the entire dive* (air or nitrox up to a maximum of 40% oxygen fraction), and *is performed within the no-decompression limits of the table or dive computer being used*.

It is generally understood by the sport diver that a direct ascent to the surface can be made at any time during the dive, notwithstanding the recommended practice of safety stops. Such ascents typically create large and rapid gradients between the dissolved gas tension in the diver's body and the ambient pressure in the surrounding medium.

Because high-oxygen mixtures are not available to accelerate off-gassing and reduce gradients, problems associated with gas loading become more severe as the depth and/or duration of the dive increase.

Technical diving. A major instigator of this on-going revolution in sport-diving practice was the now defunct magazine *AquaCorps*, which, from 1991 through 1995, published articles that addressed such technical topics as decompression theory, deep diving, and mixed-gas breathing--topics that far exceeded the interests and comprehension of most sport divers.

Hamilton used the term *technical diver* in the very first issue of *AquaCorps:* More recently, noting that the term was originally used by the British Royal Navy for rebreather diving, he has redefined *technical diving* as *diving with more than one breathing gas or with a rebreather* (Hamilton 1999). Pyle defines a *technical diver* (Pyle 1999b) as *anyone who routinely conducts dives with staged stops during an ascent as suggested by a given decompression algorithm*.

References

Albano, G. 1970. *Principles and Observations on the Physiology of the Scuba Diver*, English translation: ONR Report DR-150, Office of Naval Research, Department of the Navy, Arlington, Virginia.

Baker, E.C. 1998a. Understanding M-values. Immersed. Vol. 3, No. 3, 23-27.

Baker, E.C. 1998b. Clearing up the confusion about deep stops. Immersed. Vol. 3, No. 4, 23-31.

Bühlmann, A.A. 1995. *Tauchmedizin*. Springer-Verlag, Berlin.

Cowley, J.R.M., Allegra, C., and Lambertsen, C.J. 1979. Measurement of subcutaneous tissue pressure during superficial isobaric gas counter-diffusion. J. Appl. Physiol.:Respir. Environ. Exercise Physiol. 47:224-227.

Gerth, W.A. and Hemmingsen, E.A. 1976. Gas supersaturation thresholds for spontaneous cavitation in water with gas equilibration pressures up to 570 atm. Z. Naturforsch. 31A:1711-1716.

Hamilton, R.W. 1999. Private communication to the Decompression List dated October 4, 1999.

Harvey, E.N., Barnes, D.K., McElroy, W.D., Whiteley, A.H., Pease, D.C., and Cooper, K.W. 1944. Bubble formation in animals. I. Physical factors. J. Cell. Comp. Physiol. 24:1-22.

Hennessy, T.R. and Hempleman H.V. 1977. An examination of the critical released gas volume concept in decompression sickness. Proc. R. Soc. Lond. B. 197:299-313.

Hills, B.A. 1966. *A thermodynamic and kinetic approach to decompression sickness*. Doctoral thesis, The university of Adelaide, Australia.

Hills, B.A. 1977. *Decompression Sickness*. John Wiley and Sons, Inc., New York.

Jablonski, J. and Baker, E.C. 1999. Taking cave diving to the limit. Immersed. Vol. 4, No. 3, 29-33.

Kidd, D.J., Stubbs, R.A., and Weaver, R.S. 1971. Comparative approaches to prophylactic decompression. In: Lambertsen, C.J., ed. *Underwater physiology: Proceedings of the fourth symposium on underwater physiology*. Academic Press, New York, 167-177.

Kozlov, M.M. and Markin, V.S. 1990. Elastic properties of membranes: monolayers, bilayers, vesicles. J. Colloid Interface Sci. 138:332-345.

LeMessurier, D.H. and Hills, B.A. 1965. Decompression Sickness: A Study of Diving Techniques in the Torres Strait. Hvaldradets Skrifter 48:54-84.

Maiken, E.B. 1995. "Bubble Decompression Strategies." *tek95* Diving Technology Conference.

Pyle, R.L. 1996. The Importance of Deep Safety Stops: Rethinking Ascent Patterns From Decompression Dives. DeepTech 5:64.

Pyle, R. 1999a. Private communication to the Decompression List dated September 29, 1999.

Pyle, R. 1999b. Private communication to the Decompression List dated October 4, 1999.

Royal Naval Physiological Laboratory. 1968. *Air Diving Tables*. Her Majesty's Stationary Office, London.

Schreiner, H.R. and Kelley, P.L. 1971. A pragmatic view of decompression. In: Lambertsen, C.J., ed. *Underwater physiology: Proceedings of the fourth symposium on underwater physiology*. Academic Press, New York, 205-219.

U.S. Department of the Navy. 1977. *U.S. Navy Diving Manual* (NAVSHIPS 0994-LP-001-9010). U.S. Government Printing Office, Washington.

Wienke, B.R. 1991. *Basic Decompression Theory and Application*. Best Publishing Co., Flagstaff, Arizona.

Workman, R.D. 1965. Calculation of decompression schedules for nitrogen-oxygen and helium-oxygen dives. Research Report 6-65. U.S. Navy Experimental Diving Unit, Washington, D.C.

Yount, D.E. 1979a. Skins of varying permeability: a stabilization mechanism for gas cavitation nuclei. J. Acoust. Soc. Am. 65:1429-1439.

Yount, D.E. 1979b. Application of a bubble formation model to decompression sickness in rats and humans. Aviat. Space Environ. Med. 50:44-50.
Yount, D.E. 1979c. Multiple inert-gas bubble disease: a review of the theory. In: Lambertsen, C.J. and Bornmann, R.C. eds. *Isobaric Inert Gas Counterdiffusion*. Undersea Medical Society, Bethesda, 90-125.
Yount, D.E. 1982. On the evolution, generation, and regeneration of gas cavitation nuclei. J. Acoust. Soc. Am. 71:1473-1481.
Yount, D.E., Gillary, E.W., and Hoffman, D.C. 1984. A microscopic investigation of bubble formation nuclei. J. Acoust. Soc. Am. 76:1511-1521.
Yount, D.E. and Hoffman, D.C. 1983. Decompression theory: a dynamic critical-volume hypothesis. In: Bachrach A.J. and Matzen, M.M. eds. *Underwater physiology VIII: Proceedings of the eighth symposium on underwater physiology*. Undersea Medical Society, Bethesda, 131-146.
Yount, D.E. and Hoffman, D.C. 1986. On the use of a bubble formation model to calculate diving tables. Aviat. Space Environ. Med. 57:149-156.
Yount, D.E. and Hoffman, D.C. 1989. On the use of a bubble formation model to calculate nitrogen and helium diving tables. In: Paganelli, C.V. and Farhi, L.E. eds. *Physiological functions in special environments*. Springer-Verlag, New York, 95-108.
Yount, D.E., Kunkle, T.D., D'Arrigo, J.S., Ingle, F.W., Yeung, C.M., and Beckman, E.L. (1977). Stabilization of gas cavitation nuclei by surface-active compounds. Aviat. Space Environ. Med. 48:185-191.
Yount, D.E. and Strauss, R.H. 1976. Bubble formation in gelatin: A model for decompression sickness. J. Appl. Phys. 47:5081-5089.
Yount, D.E. and Yeung, C.M. 1981. Bubble formation in supersaturated gelatin: a further investigation of gas cavitation nuclei. J. Acoust. Soc. Am. 69:702-708.
Yount, D.E., Yeung, C.M., and Ingle, F.W. 1979. Determination of the radii of gas cavitation nuclei by filtering gelatin. J. Acoust. Soc. Am. 65:1440-1450.

Figure Captions

1. Outline of the varying-permeability model (Yount 1982). The spherical geometry and the condition for mechanical equilibrium are illustrated in (a). A magnified view of the skin and the reservoir is shown in (b), and (c) is a plot of pressure versus radius indicating at what points the various pressures apply. The rudimentary pressure schedule in (d) consists of a rapid compression from p_o to p_m, saturation of the sample at $p_s = p_m$, and a rapid decompression from p_s to p_f.

2. The Haldane-ratio principle has been tested by exposing gelatin samples to the three schedules shown in this figure (Yount and Strauss 1976). Schedules A and B have different ratios and produce the same number of bubbles, while Schedules A and C have the same ratios and produce different numbers of bubbles. As discussed in the text, the bubble counts in gelatin depend only on the pressure differences p_{crush} and p_{ss}, and not on the Haldane ratio, p_s/p_f.

3. Stepped compression schedule used to limit the over pressure p_{crush} without affecting the supersaturation p_{ss} (Yount and Yeung 1981).

4. Plot of p_{ss} versus p_{crush} for various numbers of bubbles N (Yount and Yeung 1981). All of the points in the "old region" and many of those in the "new region" lie on a family of straight lines generated by the Varying Permeability Model.

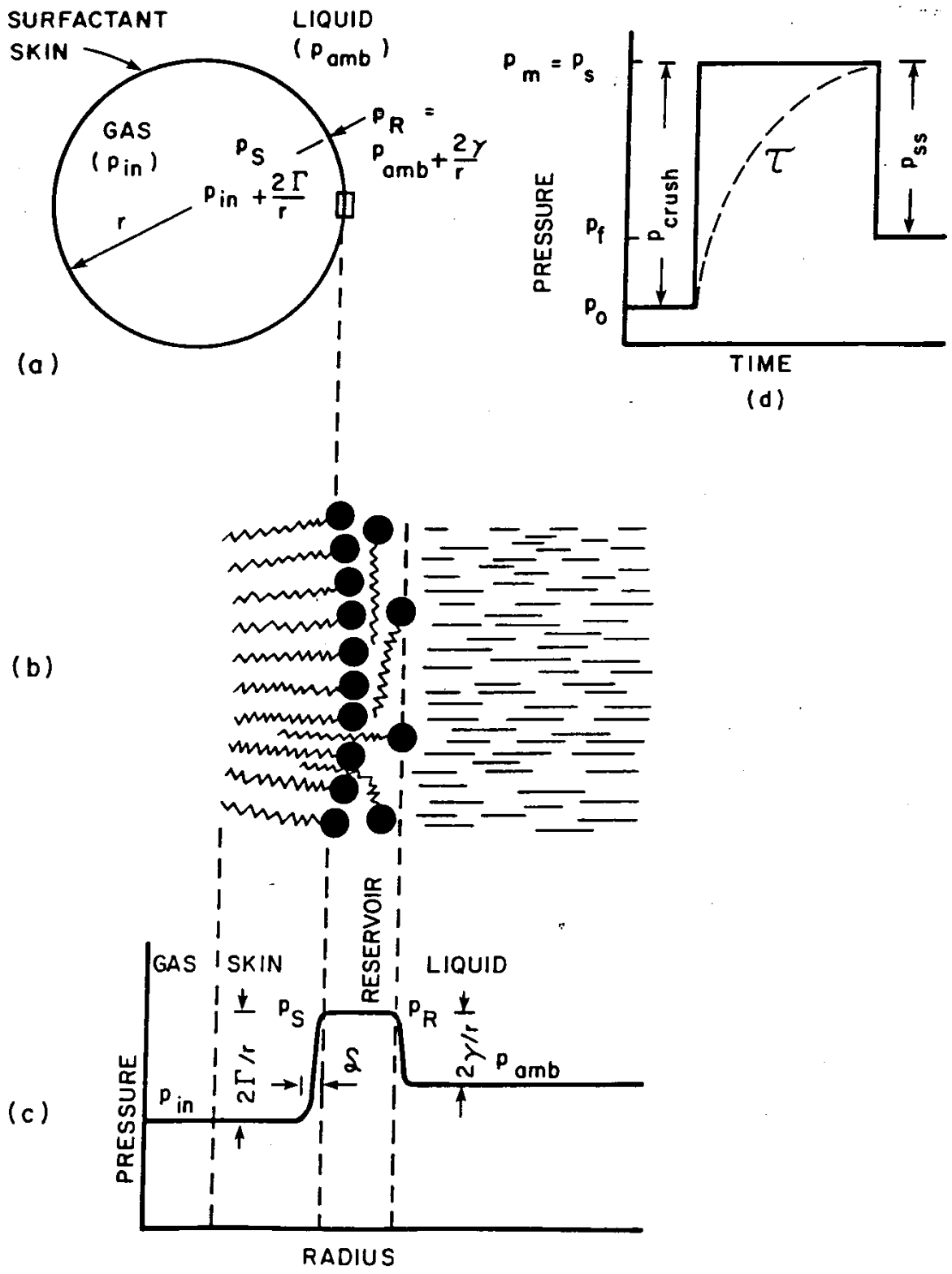

Figure 1
Yount, Maiken, Baker

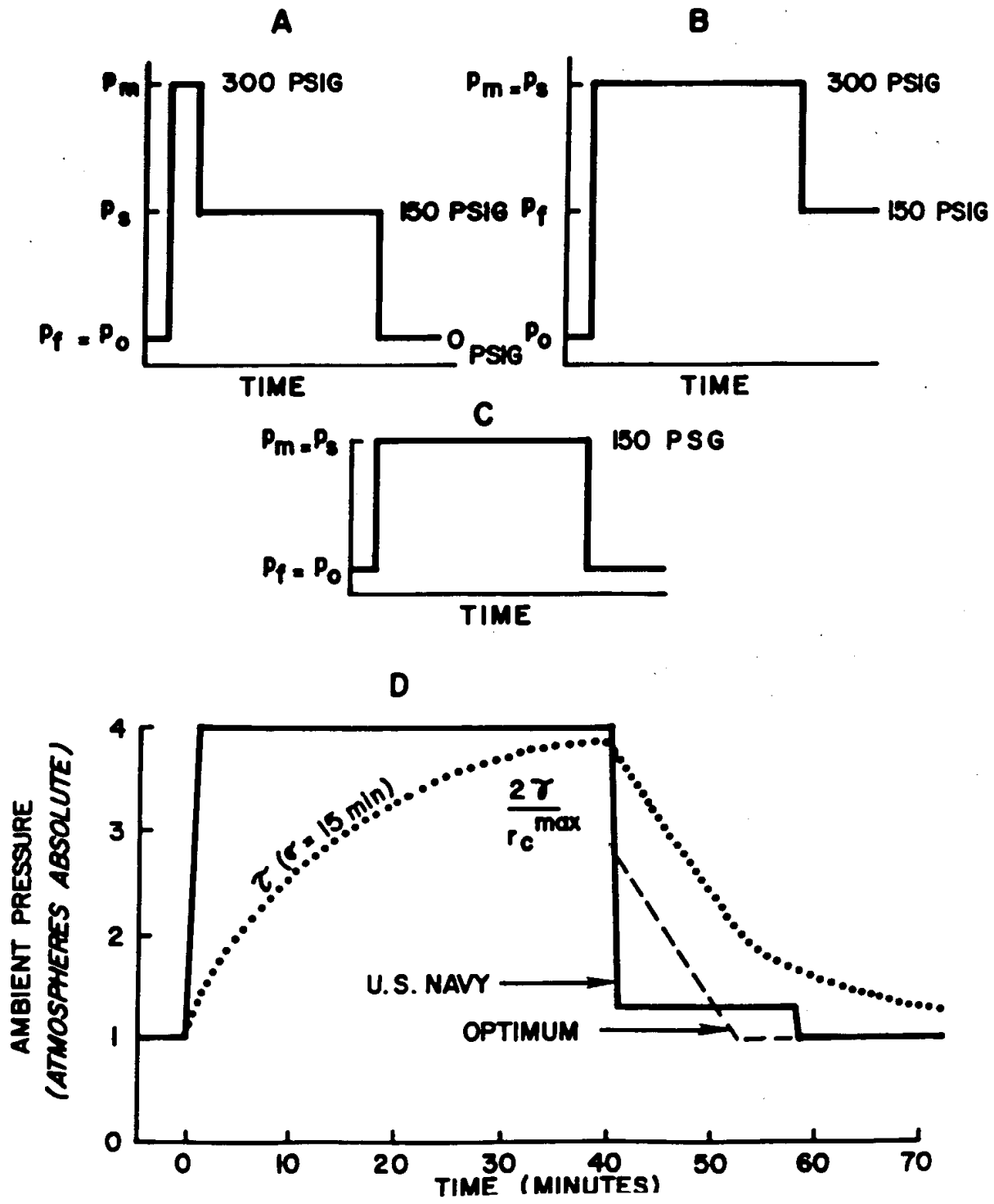

Figure 2
Yount, Maiken, Baker

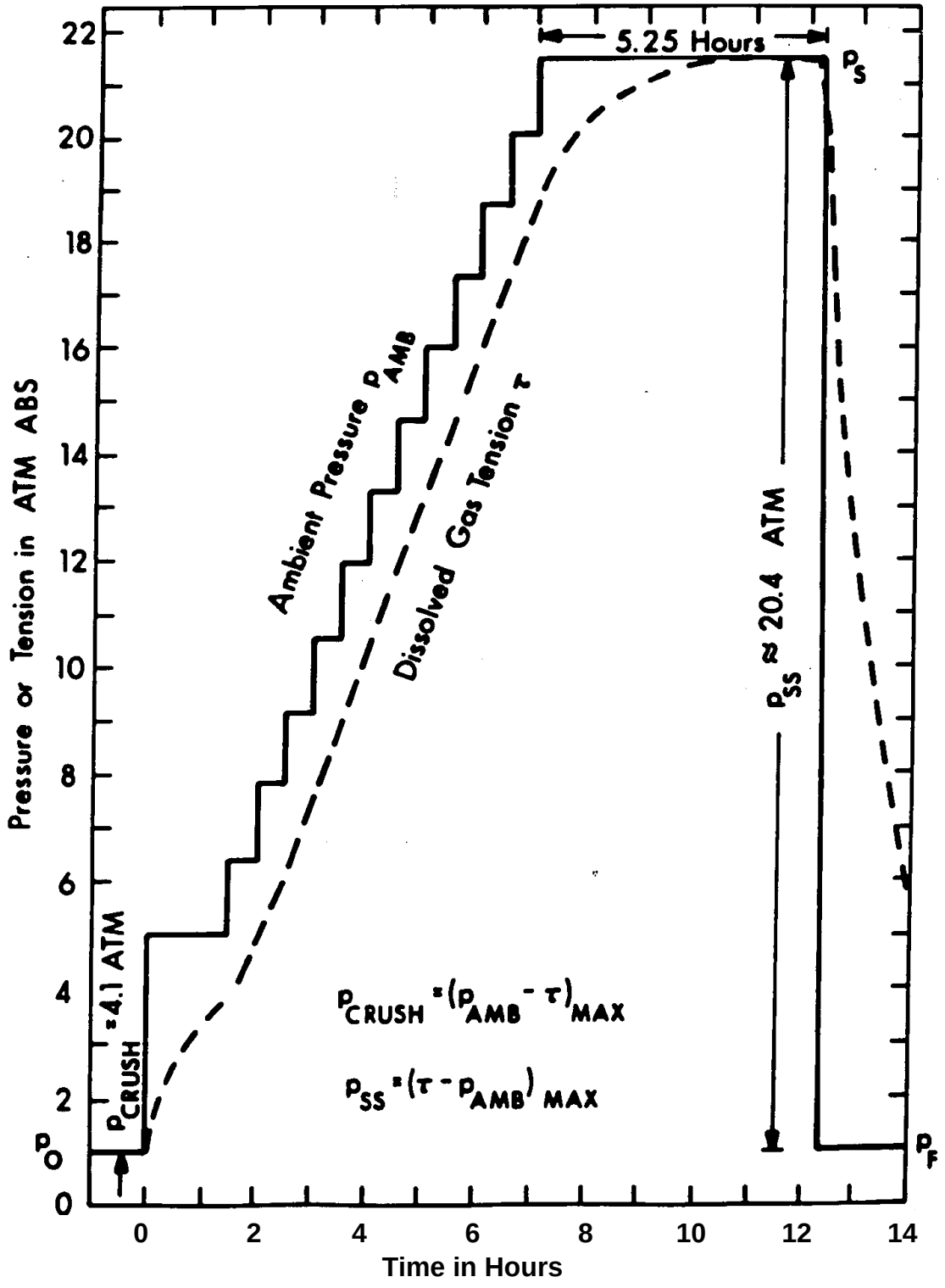

Figure 3
Yount, Maiken, Baker

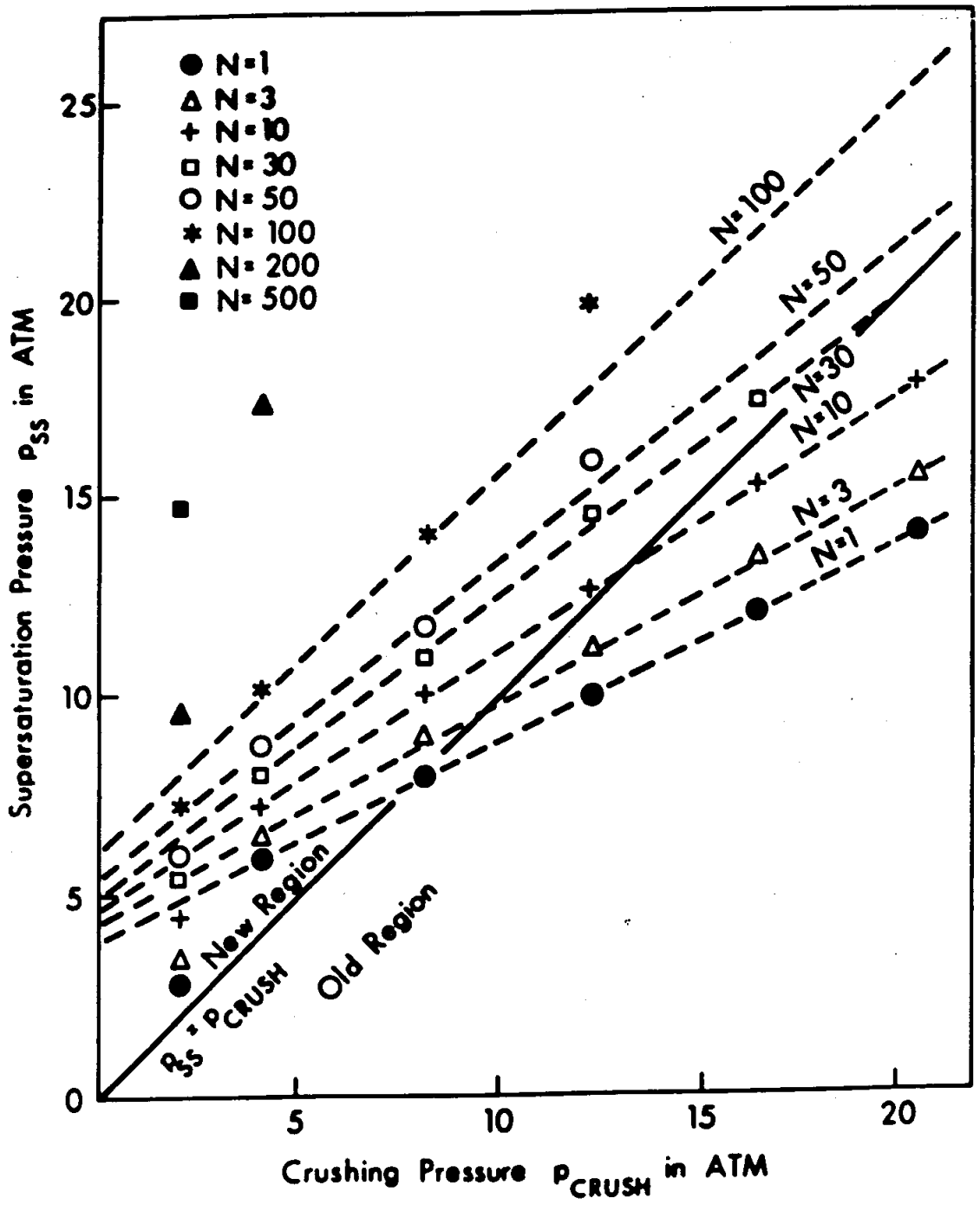

Figure 4
Yount, Maiken, Baker

Pressure Graph:

Ascent Profile For First Dive Of Reverse Dive Series 1A, 2A, and 3A
Inert Gas Loadings Versus Conventional M-values

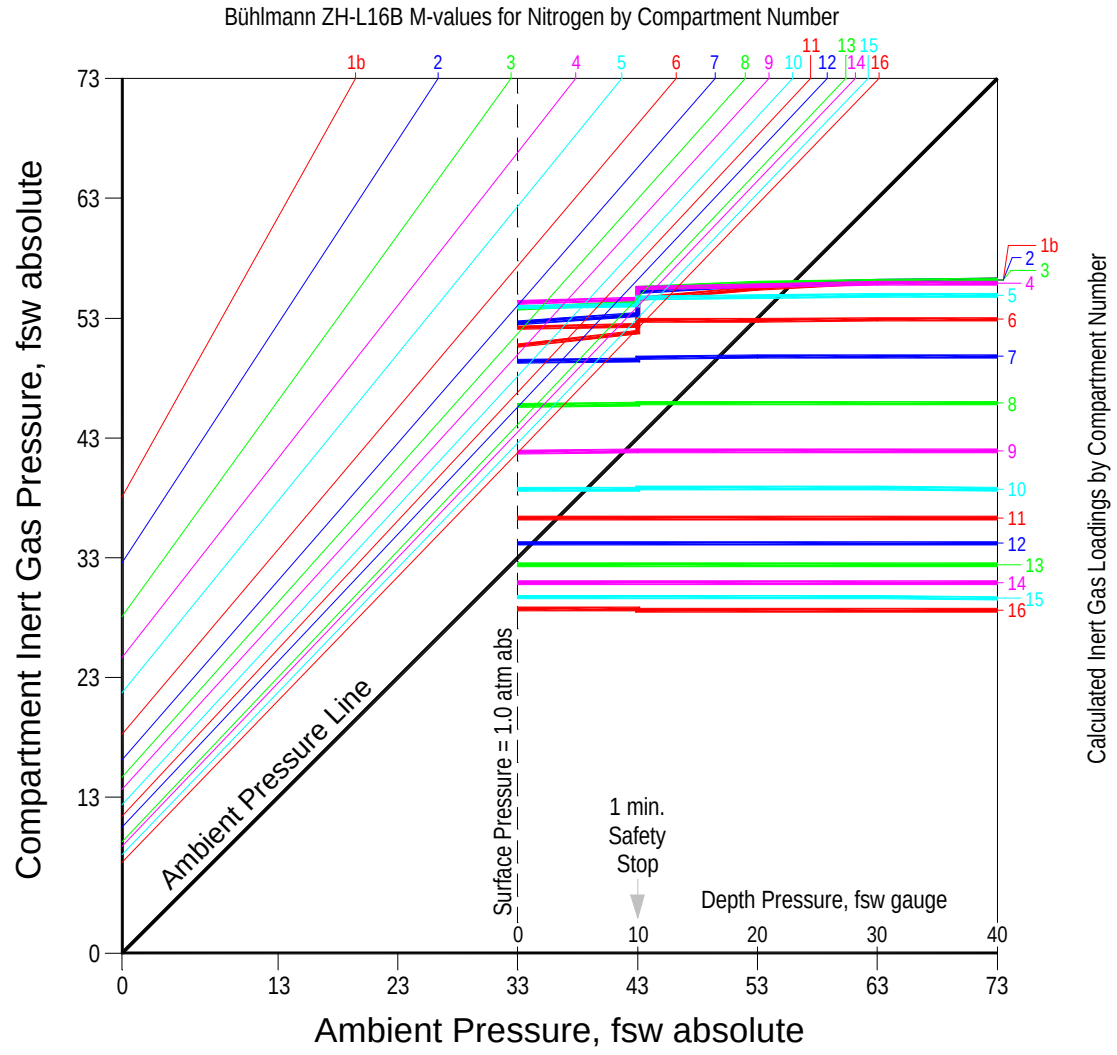

Notes:

1. Air dive to 40 fsw for 125 minutes bottom time according to no-decompression limit of Bühlmann ZH-86 Air Diving Tables.
2. Inert gas is nitrogen. Gas loadings are shown leaving the bottom at the end of the bottom time.
3. Ascent rate is 30 fsw/min. Descent rate is 75 fsw/min and descent is included in the bottom time.
4. A one minute safety stop is required for all no-deco dives according to the Bühlmann ZH-86 Air Diving Tables.

Observations:

1. M-values for fast compartments permit large overpressure gradients and thus allow profuse bubble formation.
2. Upon surfacing from this dive, Compartments 6 and 7 are leading (gas loadings closest to M-values).
3. The one minute safety stop at 10 fsw has only a mild effect in terms of dropping gas loadings.

Figure 5
Yount, Maiken, Baker

Pressure Graph:

Ascent Profile For First Dive Of Reverse Dive Series 1A, 2A, and 3A
Inert Gas Loadings Versus VPM Criterion for Bubble Formation

Shown Upon Surfacing: Lines of Fixed Gradient = Isopleths of Constant Bubble Number
Calculated Based on Minimum Initial Radius (microns) of Gas Nuclei at Start of Dive Series

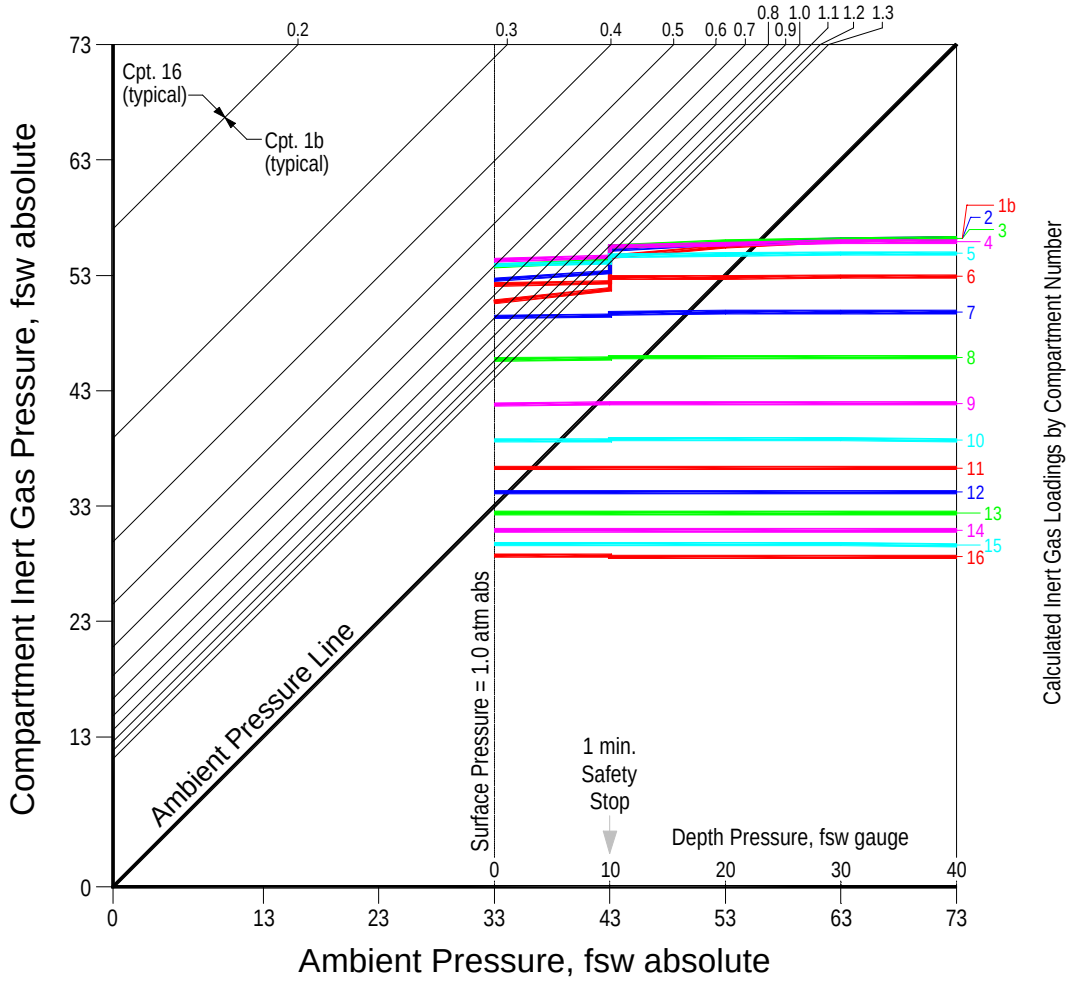

Notes:

1. Air dive to 40 fsw for 125 minutes bottom time according to no-decompression limit of Bühlmann ZH-86 Air Diving Tables.
2. Inert gas is nitrogen. Gas loadings are shown leaving the bottom at the end of the bottom time.
3. Ascent rate is 30 fsw/min. Descent rate is 75 fsw/min and descent is included in the bottom time.
4. VPM criterion is computed with varying differential crushing and supersaturation pressures across the 16 compartments.

Observations:

1. Bubbles are formed in Compartments 1b thru 7 upon surfacing from this dive.
2. Overpressure (supersaturation) gradients will exist for up to 60 minutes after this dive to drive bubble growth.
3. A surface interval of less than 60 minutes after this first dive could carry free-phase gas over into a repetitive dive as bubbles or gas nuclei with larger initial radius.

Figure 6
Yount, Maiken, Baker

Pressure Graph:

Ascent Profile For Repetitive Dive Of Reverse Dive Series 1A
Inert Gas Loadings Versus Conventional M-values

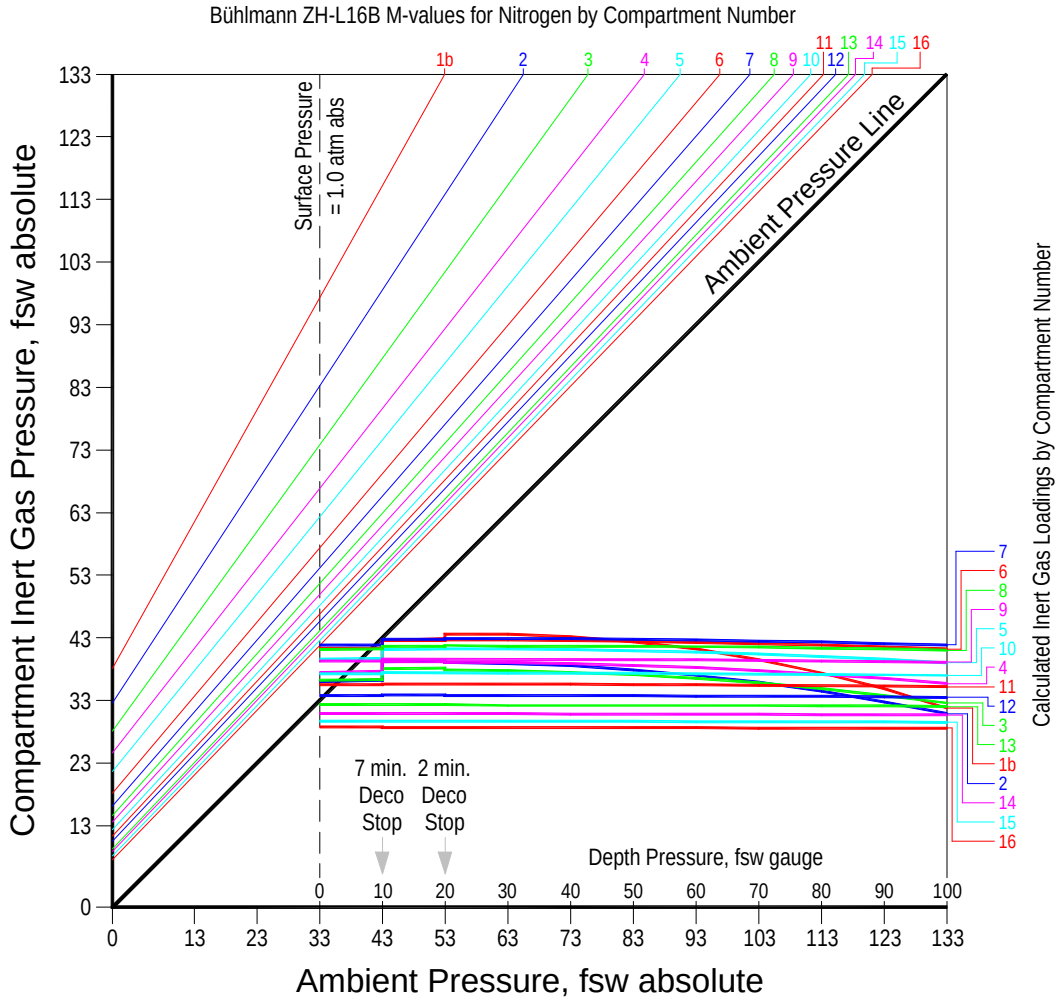

Notes:

1. After surface interval of 30 minutes, repetitive air dive to 100 fsw followed by immediate ascent (spike dive).
2. Inert gas is nitrogen. Gas loadings are shown leaving the bottom at the end of the bottom time.
3. Ascent rate is 30 fsw/min. Descent rate is 75 fsw/min and the bottom time is only momentary.
4. Due to residual nitrogen loading, deco stops are required at 20 and 10 fsw per Bühlmann ZH-86 Air Diving Tables.

Observations:

1. Gas loadings are well clear of M-values throughout ascent. No significant on-gassing during this dive.
2. Upon surfacing from this dive, Compartments 8 and 9 are leading (gas loadings closest to M-values).
3. It does not appear that there should be any problems following this dive unless free-phase gas (bubbles or large nuclei) carried over to this dive from the first dive.

Figure 7
Yount, Maiken, Baker

Pressure Graph:

Ascent Profile For Repetitive Dive Of Reverse Dive Series 1A
Inert Gas Loadings Versus VPM Criterion for Bubble Formation

Shown Upon Surfacing: Lines of Fixed Gradient = Isopleths of Constant Bubble Number
Calculated Based on Minimum Initial Radius (microns) of Gas Nuclei at Start of Dive Series

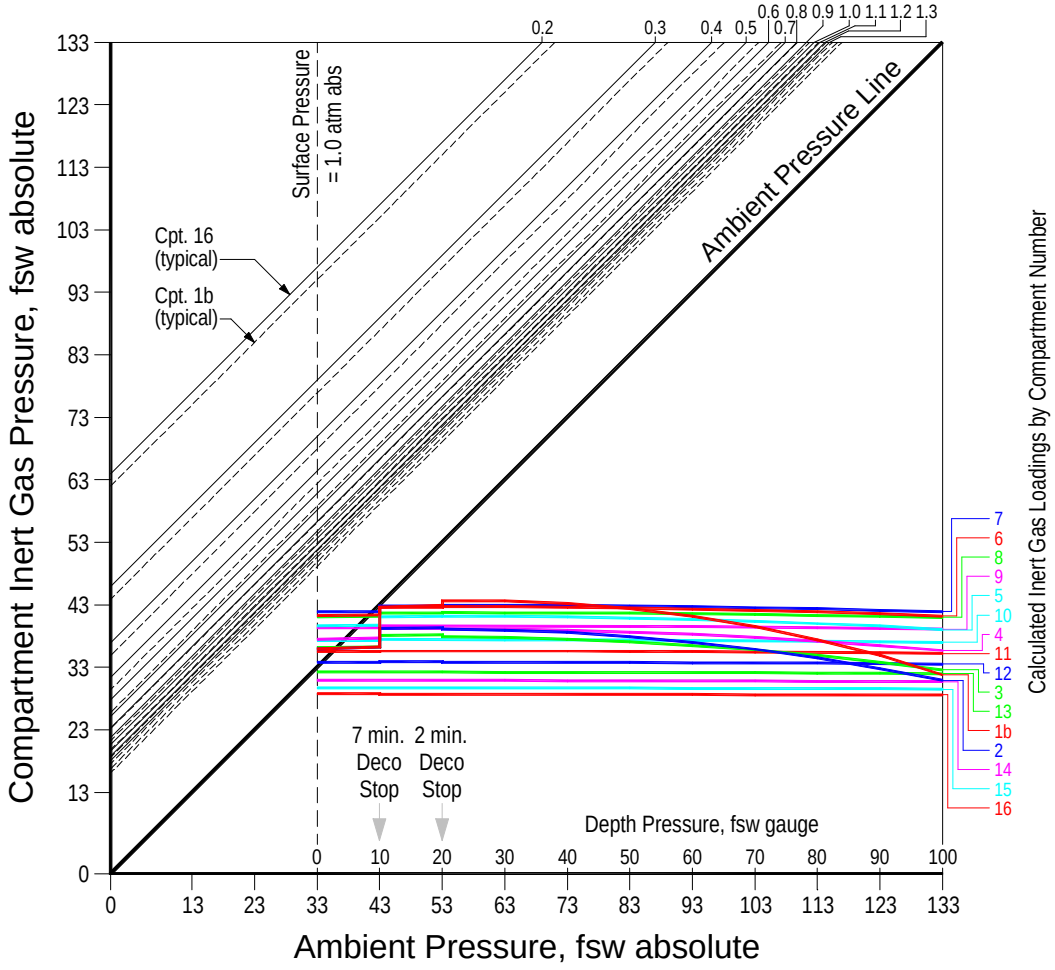

Notes:

1. After surface interval of 30 minutes, repetitive air dive to 100 fsw followed by immediate ascent (spike dive).
2. Inert gas is nitrogen. Gas loadings are shown leaving the bottom at the end of the bottom time.
3. Ascent rate is 30 fsw/min. Descent rate is 75 fsw/min and the bottom time is only momentary.
4. VPM criterion is computed with varying differential crushing and supersaturation pressures across the 16 compartments.

Observations:

1. No bubbles are formed as a result of the repetitive dive.
2. It does not appear that there should be any problems following this dive unless free-phase gas (bubbles or large nuclei) carried over to this dive from the first dive.

Figure 8
Yount, Maiken, Baker

Pressure Graph:

Ascent Profile For Repetitive Dive Of Reverse Dive Series 2A
Inert Gas Loadings Versus Conventional M-values

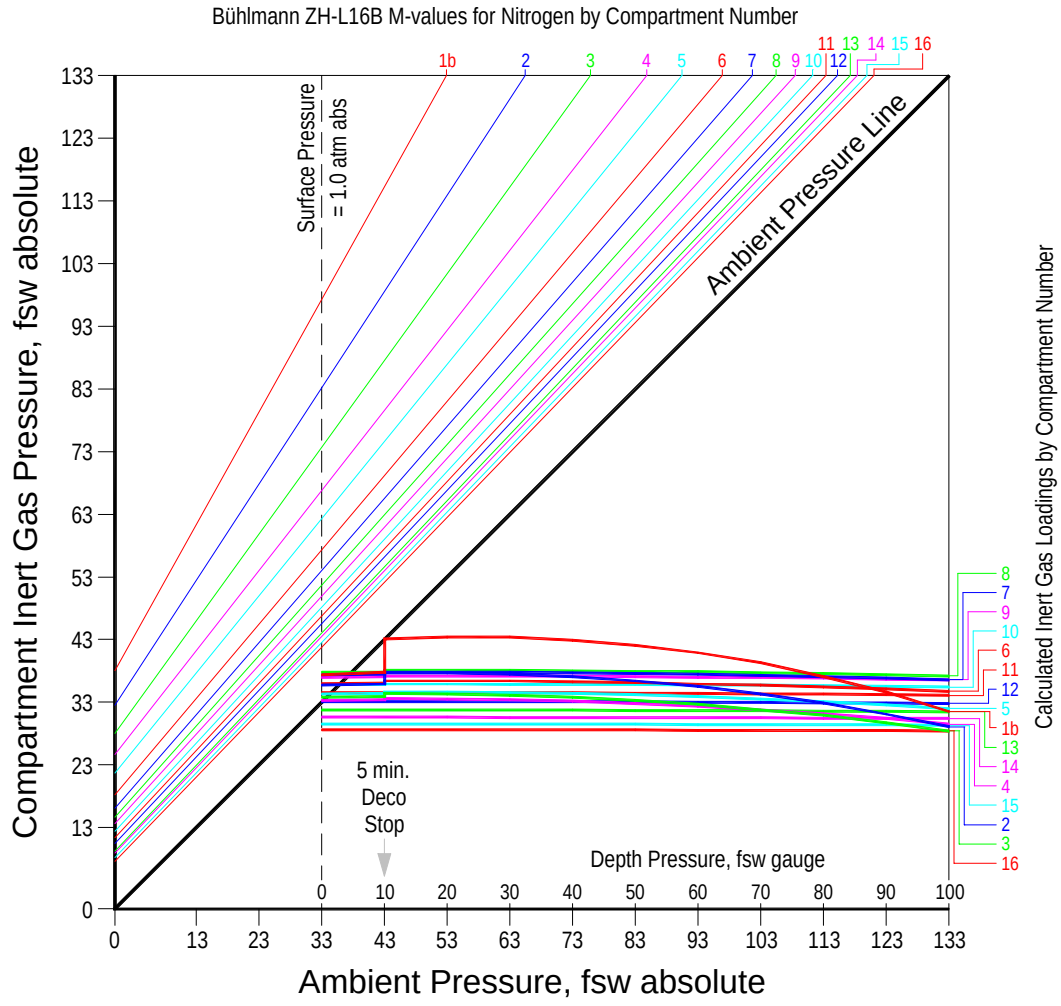

Notes:

1. After surface interval of 60 minutes, repetitive air dive to 100 fsw followed by immediate ascent (spike dive).
2. Inert gas is nitrogen. Gas loadings are shown leaving the bottom at the end of the bottom time.
3. Ascent rate is 30 fsw/min. Descent rate is 75 fsw/min and the bottom time is only momentary.
4. Due to residual nitrogen loading, a deco stop is required at 10 fsw per Bühlmann ZH-86 Air Diving Tables.

Observations:

1. Gas loadings are well clear of M-values throughout ascent. Noticeable on-gassing in Compartment 1b during this dive.
2. Upon surfacing from this dive, Compartments 9 and 10 are leading (gas loadings closest to M-values).
3. It does not appear that there should be any problems following this dive unless free-phase gas (bubbles or large nuclei) carried over to this dive from the first dive.

Figure 9
Yount, Maiken, Baker

Pressure Graph:

Ascent Profile For Repetitive Dive Of Reverse Dive Series 2A
Inert Gas Loadings Versus VPM Criterion for Bubble Formation

Shown Upon Surfacing: Lines of Fixed Gradient = Isopleths of Constant Bubble Number
Calculated Based on Minimum Initial Radius (microns) of Gas Nuclei at Start of Dive Series

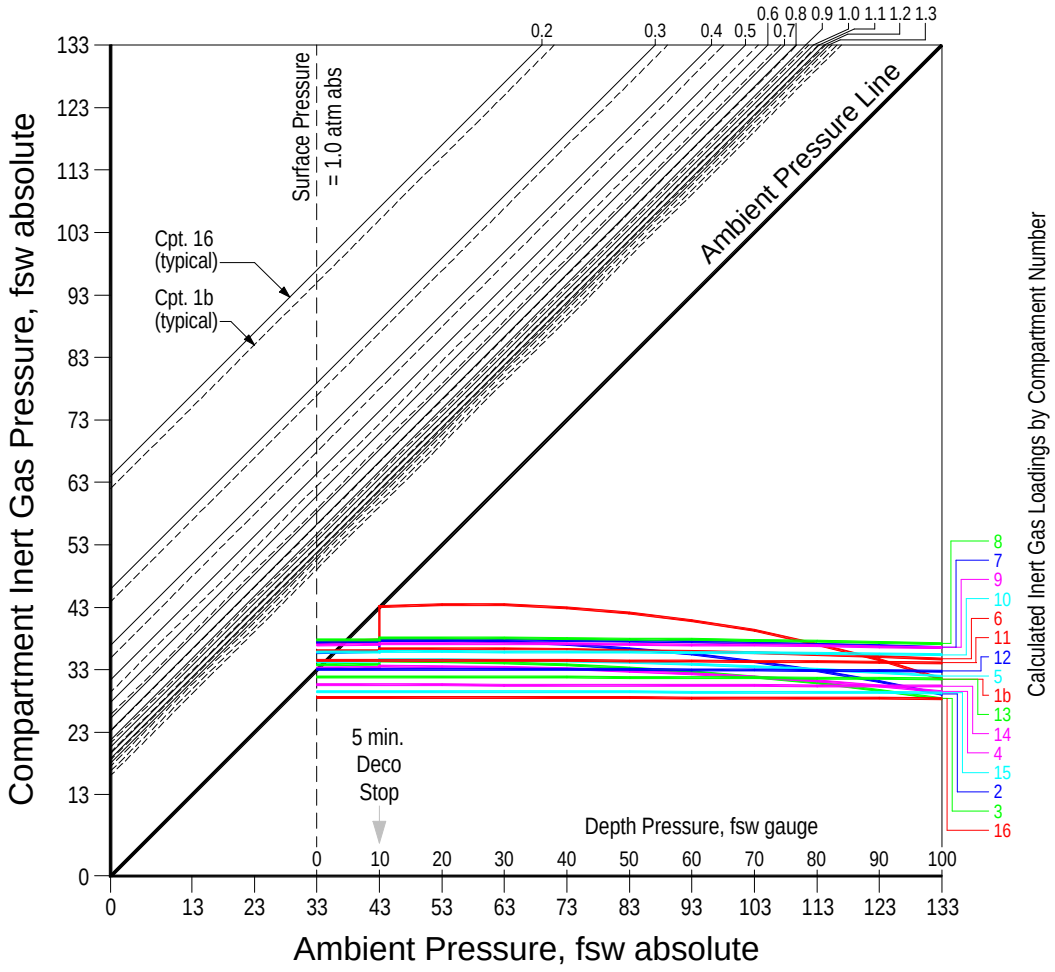

Notes:

1. After surface interval of 60 minutes, repetitive air dive to 100 fsw followed by immediate ascent (spike dive).
2. Inert gas is nitrogen. Gas loadings are shown leaving the bottom at the end of the bottom time.
3. Ascent rate is 30 fsw/min. Descent rate is 75 fsw/min and the bottom time is only momentary.
4. VPM criterion is computed with varying differential crushing and supersaturation pressures across the 16 compartments.

Observations:

1. No bubbles are formed as a result of the repetitive dive.
2. It does not appear that there should be any problems following this dive unless free-phase gas (bubbles or large nuclei) carried over to this dive from the first dive.

Figure 10
Yount, Maiken, Baker

Pressure Graph:

Ascent Profile For Repetitive Dive Of Reverse Dive Series 3A
Inert Gas Loadings Versus Conventional M-values

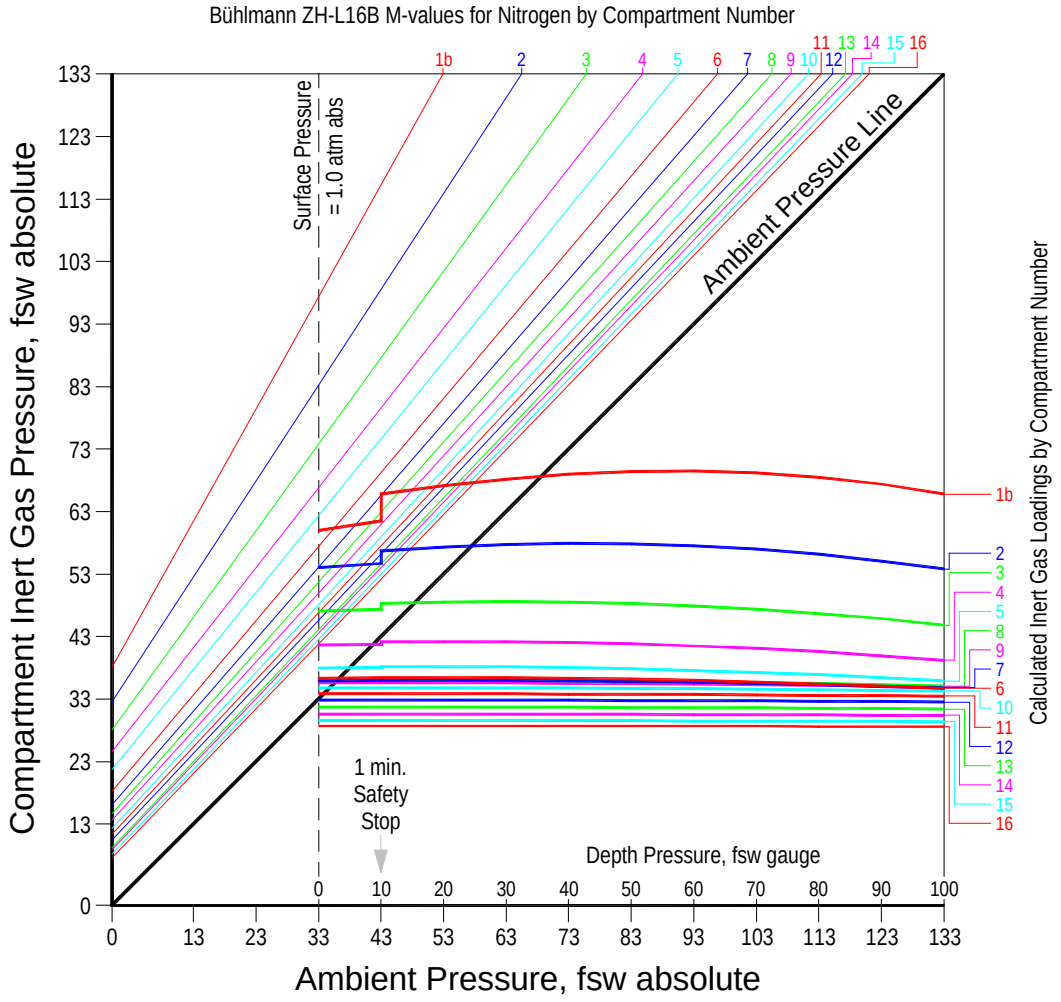

Notes:

1. After surface interval of 120 minutes, repetitive air dive to 100 fsw for 6 minutes bottom time according to no-deco limit of Bühlmann ZH-86 Air Diving Tables.
2. Inert gas is nitrogen. Gas loadings are shown leaving the bottom at the end of the bottom time.
3. Ascent rate is 30 fsw/min. Descent rate is 75 fsw/min and descent is included in the bottom time.
4. A one minute safety stop is required by the table.

Observations:

1. M-values for fast compartments permit large overpressure gradients and thus allow profuse bubble formation.
2. Upon surfacing from this dive, Compartments 10 and 11 are leading (gas loadings closest to M-values).
3. The one minute safety stop at 10 fsw has only a mild effect in terms of dropping gas loadings.

Figure 11
Yount, Maiken, Baker

Pressure Graph:

Ascent Profile For Repetitive Dive Of Reverse Dive Series 3A
Inert Gas Loadings Versus VPM Criterion for Bubble Formation

Shown Upon Surfacing: Lines of Fixed Gradient = Isopleths of Constant Bubble Number
Calculated Based on Minimum Initial Radius (microns) of Gas Nuclei at Start of Dive Series

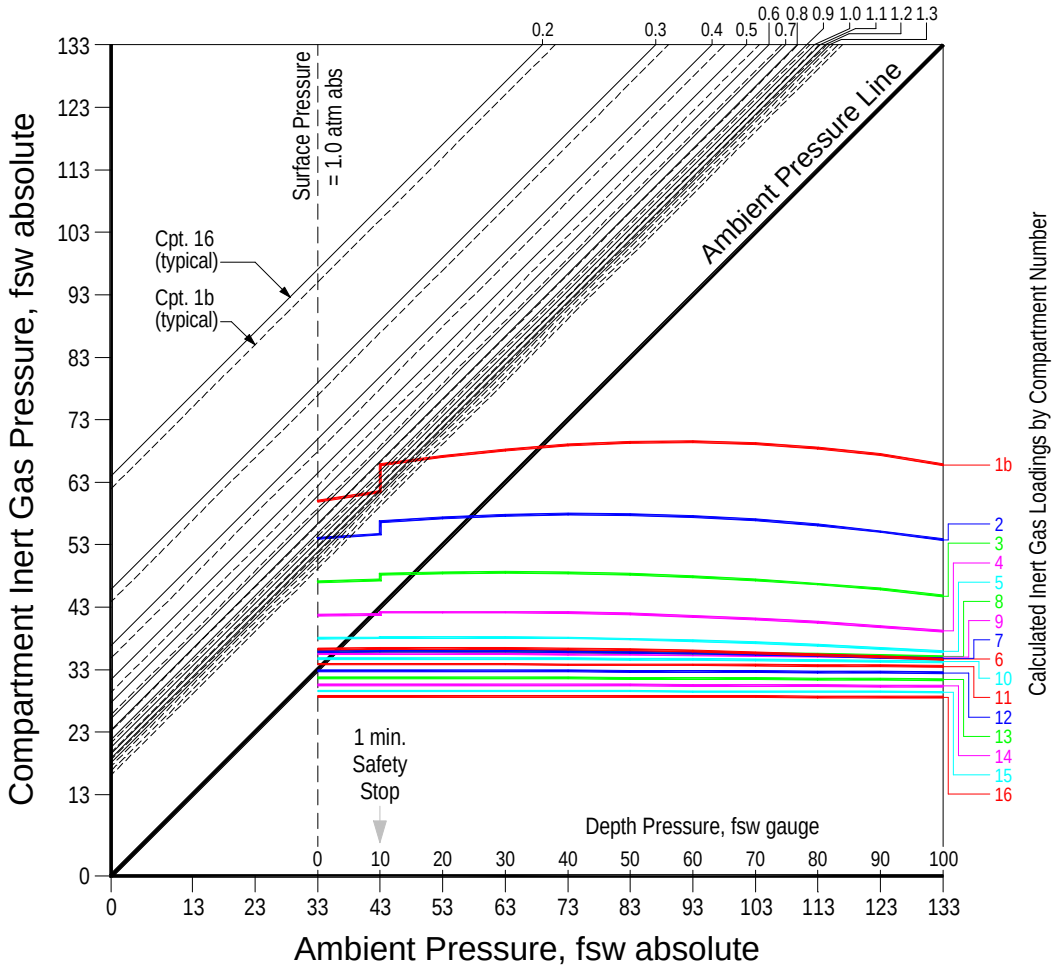

Notes:

1. After surface interval of 120 minutes, repetitive air dive to 100 fsw for 6 minutes bottom time (no-deco limit).
2. Inert gas is nitrogen. Gas loadings are shown leaving the bottom at the end of the bottom time.
3. Ascent rate is 30 fsw/min. Descent rate is 75 fsw/min and descent is included in the bottom time.
4. VPM criterion is computed with varying differential crushing and supersaturation pressures across the 16 compartments.

Observations:

1. Bubbles are formed in Compartments 1 and 2 upon surfacing from this dive.
2. Overpressure (supersaturation) gradients will exist for more than 10 minutes after this dive to drive bubble growth.

Figure 12
Yount, Maiken, Baker

Pressure Graph:

Ascent Profile For First Dive Of Forward Dive Series 1B, 2B, and 3B
Inert Gas Loadings Versus Conventional M-values

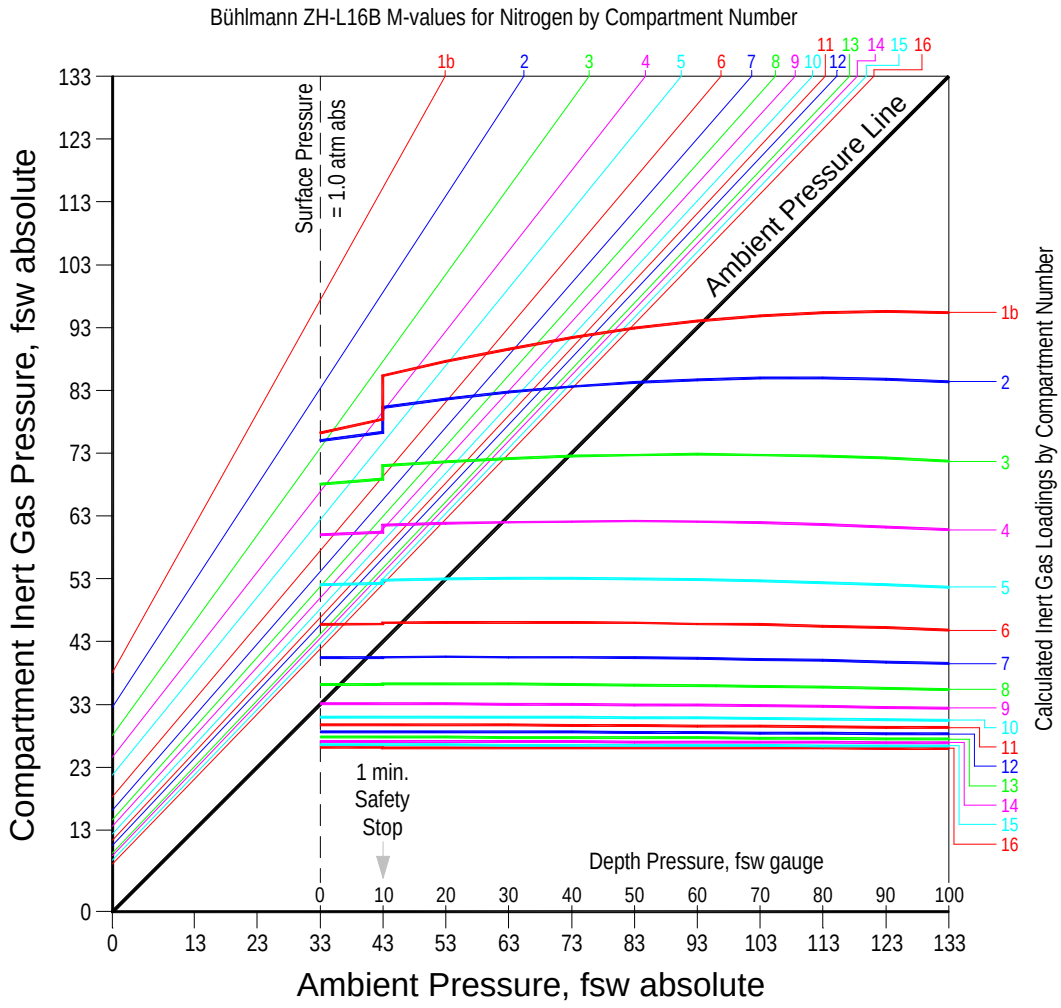

Notes:

1. Air dive to 100 fsw for 17 minutes bottom time according to no-decompression limit of Bühlmann ZH-86 Air Diving Tables.
2. Inert gas is nitrogen. Gas loadings are shown leaving the bottom at the end of the bottom time.
3. Ascent rate is 30 fsw/min. Descent rate is 75 fsw/min and descent is included in the bottom time.
4. A one minute safety stop is required for all no-deco dives according to the Bühlmann ZH-86 Air Diving Tables.

Observations:

1. M-values for fast compartments permit large overpressure gradients and thus allow profuse bubble formation.
2. Upon surfacing from this dive, Compartments 2 and 3 are leading (gas loadings closest to M-values).
3. The one minute safety stop at 10 fsw has a moderate effect in terms of dropping gas loadings.

Figure 13
Yount, Maiken, Baker

Pressure Graph:

Ascent Profile For First Dive Of Forward Dive Series 1B, 2B, and 3B
Inert Gas Loadings Versus VPM Criterion for Bubble Formation

Shown Upon Surfacing: Lines of Fixed Gradient = Isopleths of Constant Bubble Number
Calculated Based on Minimum Initial Radius (microns) of Gas Nuclei at Start of Dive Series

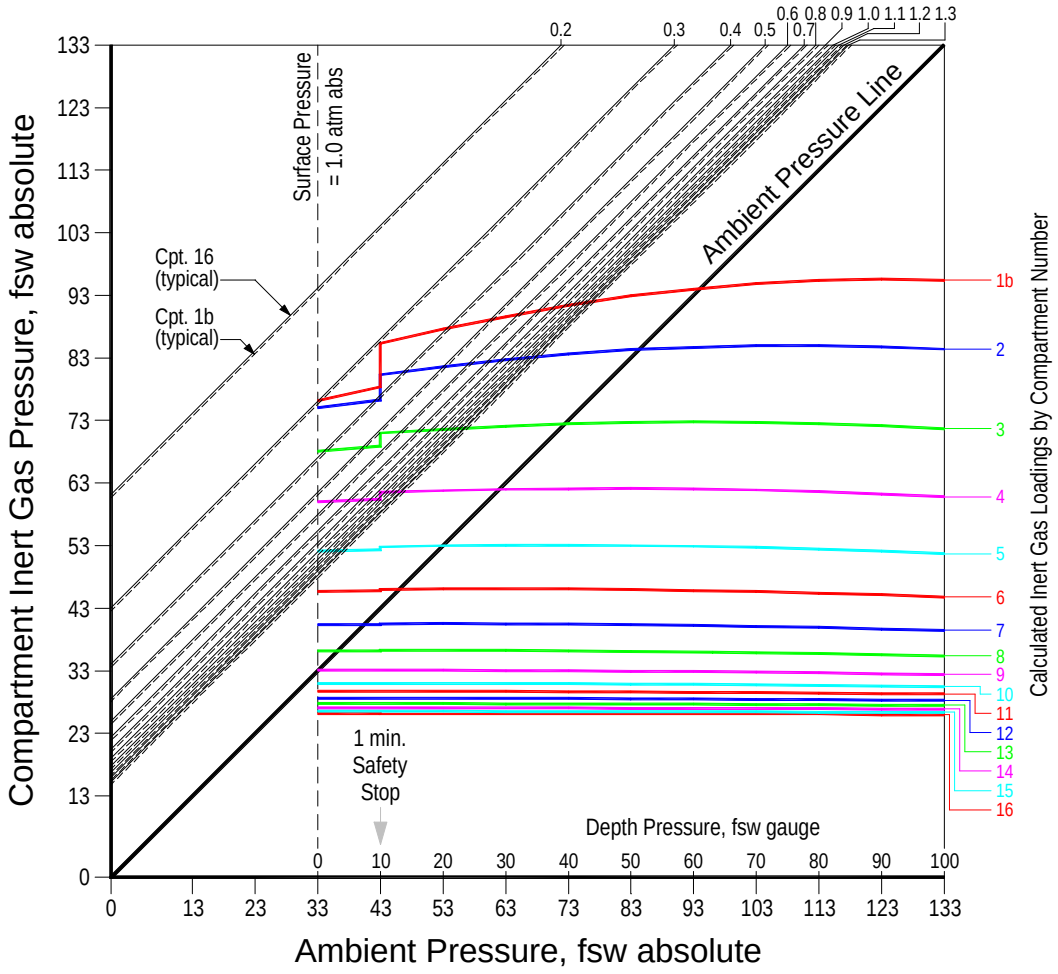

Notes:

1. Air dive to 100 fsw for 17 minutes bottom time according to no-decompression limit of Bühlmann ZH-86 Air Diving Tables.
2. Inert gas is nitrogen. Gas loadings are shown leaving the bottom at the end of the bottom time.
3. Ascent rate is 30 fsw/min. Descent rate is 75 fsw/min and descent is included in the bottom time.
4. VPM criterion is computed with varying differential crushing and supersaturation pressures across the 16 compartments.

Observations:

1. Bubbles are formed in Compartments 1b thru 5 upon surfacing from this dive.
2. Overpressure (supersaturation) gradients will exist for more than 30 minutes after this dive to drive bubble growth.
3. A surface interval of less than 30 minutes after this first dive could carry free-phase gas over into a repetitive dive as bubbles or gas nuclei with larger initial radius.

Figure 14
Yount, Maiken, Baker

Pressure Graph:

Ascent Profile For Repetitive Dive Of Forward Dive Series 1B
Inert Gas Loadings Versus Conventional M-values

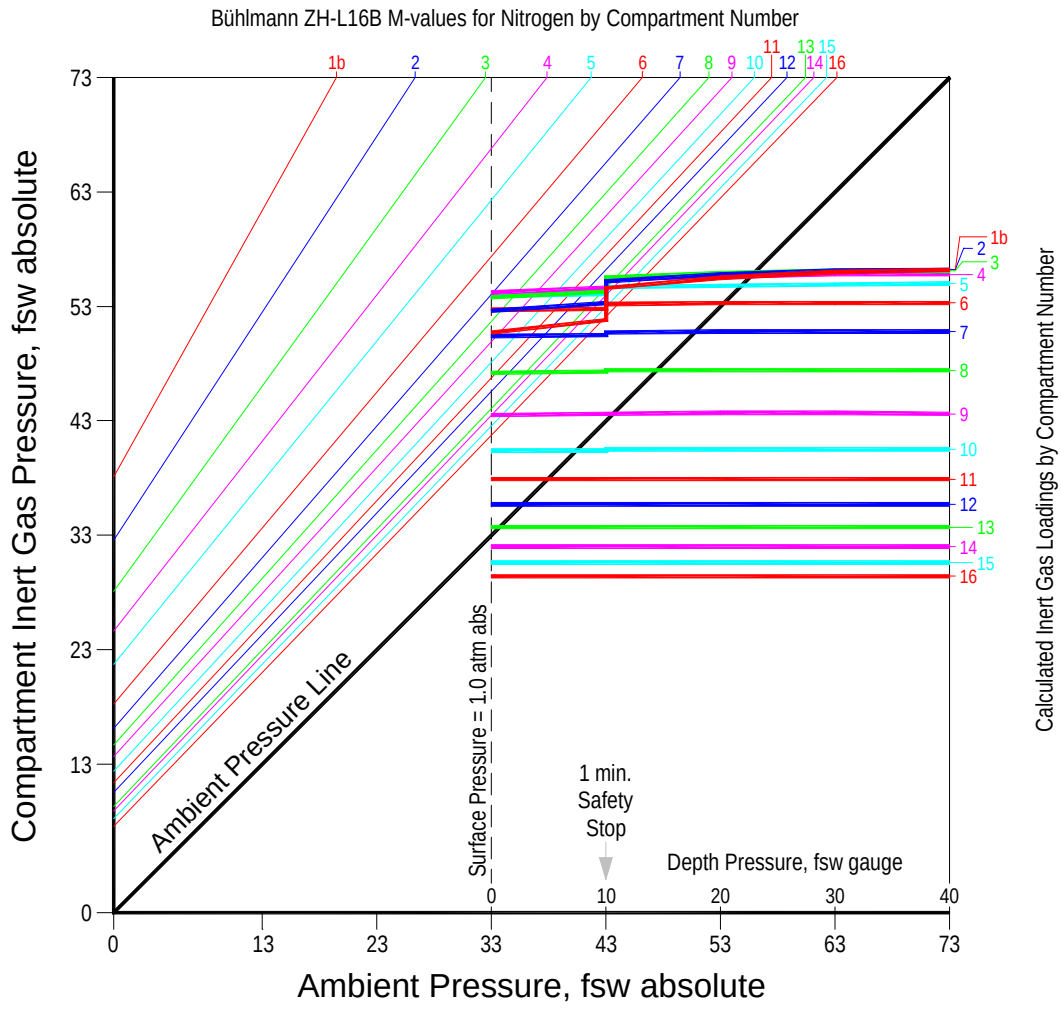

Notes:

1. After surface interval of 30 minutes, repetitive air dive to 40 fsw for 106 minutes bottom time according to no-deco limit of Bühlmann ZH-86 Air Diving Tables.
2. Inert gas is nitrogen. Gas loadings are shown leaving the bottom at the end of the bottom time.
3. Ascent rate is 30 fsw/min. Descent rate is 75 fsw/min and descent is included in the bottom time.
4. A one minute safety stop is required by the table.

Observations:

1. M-values for fast compartments permit large overpressure gradients and thus allow profuse bubble formation.
2. Upon surfacing from this dive, Compartments 6 and 7 are leading (gas loadings closest to M-values).
3. The one minute safety stop at 10 fsw has only a mild effect in terms of dropping gas loadings.

Figure 15
Yount, Maiken, Baker

Pressure Graph:

Ascent Profile For Repetitive Dive Of Forward Dive Series 1B
Inert Gas Loadings Versus VPM Criterion for Bubble Formation

Shown Upon Surfacing: Lines of Fixed Gradient = Isopleths of Constant Bubble Number
Calculated Based on Minimum Initial Radius (microns) of Gas Nuclei at Start of Dive Series

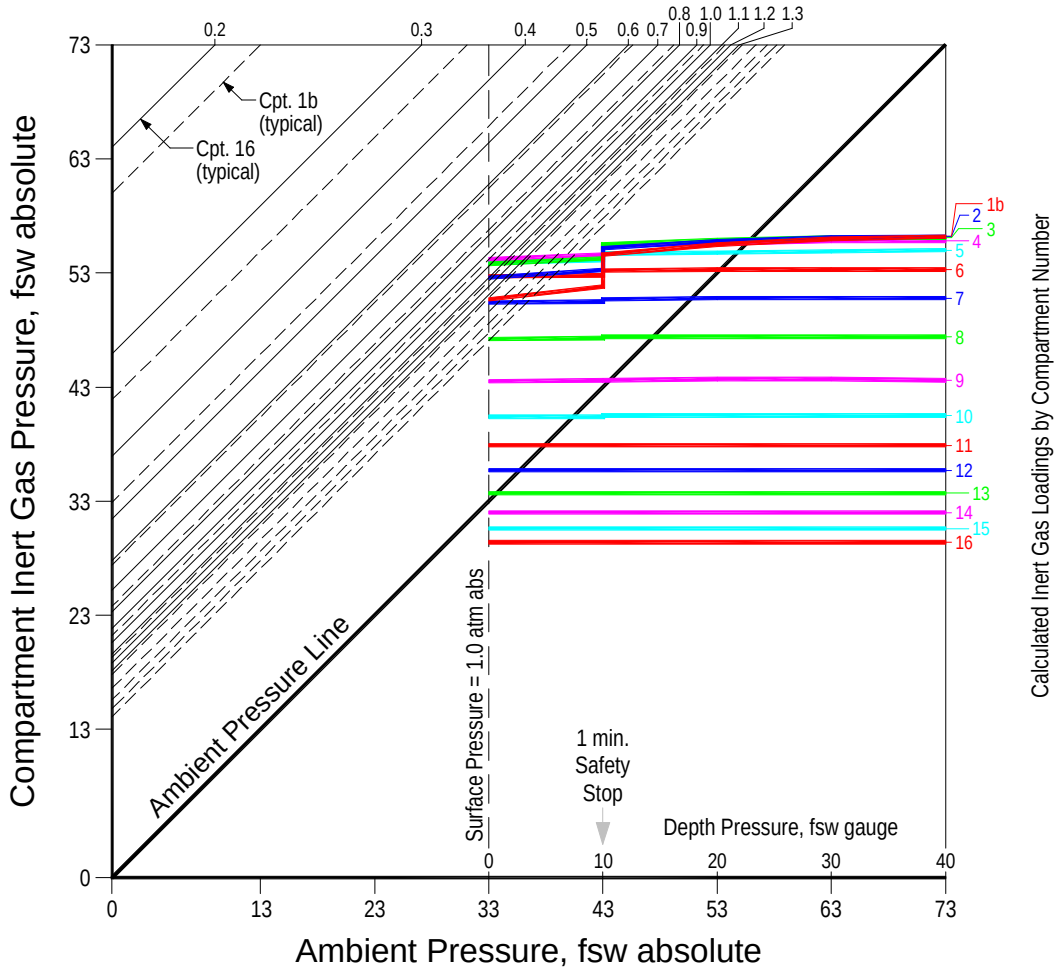

Notes:

1. After surface interval of 30 minutes, repetitive air dive to 40 fsw for 106 minutes bottom time (no-deco limit).
2. Inert gas is nitrogen. Gas loadings are shown leaving the bottom at the end of the bottom time.
3. Ascent rate is 30 fsw/min. Descent rate is 75 fsw/min and descent is included in the bottom time.
4. VPM criterion is computed with varying differential crushing and supersaturation pressures across the 16 compartments.

Observations:

1. Bubbles are formed in Compartments 1b thru 6 upon surfacing from this dive.
2. Overpressure (supersaturation) gradients will exist for over 30 minutes after this dive to drive bubble growth.
3. There is a difference of 4.0 fsw in allowable gradients between Compartments 1b and 16.

Figure 16
Yount, Maiken, Baker

Pressure Graph:

Ascent Profile For Repetitive Dive Of Forward Dive Series 2B
Inert Gas Loadings Versus Conventional M-values

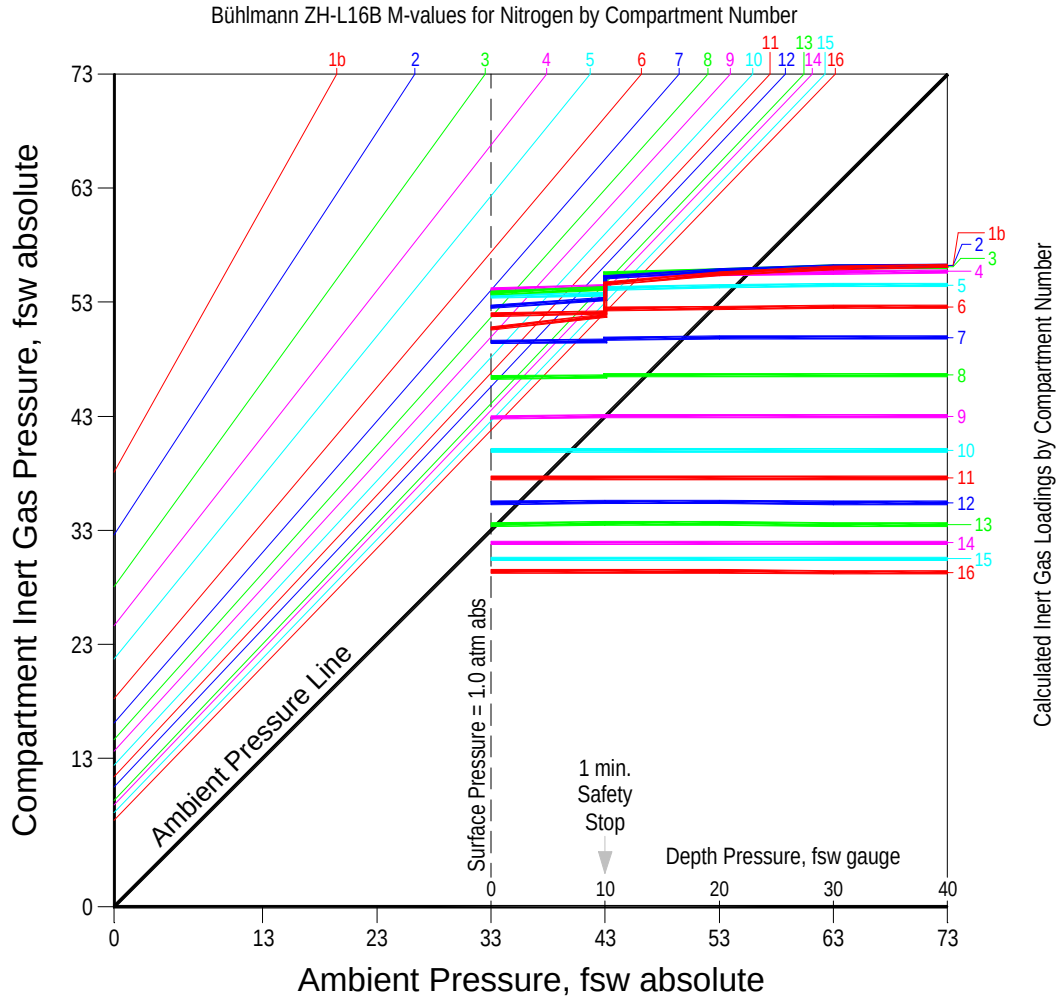

Notes:

1. After surface interval of 60 minutes, repetitive air dive to 40 fsw for 106 minutes bottom time according to no-deco limit of Bühlmann ZH-86 Air Diving Tables.
2. Inert gas is nitrogen. Gas loadings are shown leaving the bottom at the end of the bottom time.
3. Ascent rate is 30 fsw/min. Descent rate is 75 fsw/min and descent is included in the bottom time.
4. A one minute safety stop is required by the table.

Observations:

1. M-values for fast compartments permit large overpressure gradients and thus allow profuse bubble formation.
2. Upon surfacing from this dive, Compartments 6 and 7 are leading (gas loadings closest to M-values).
3. The one minute safety stop at 10 fsw has only a mild effect in terms of dropping gas loadings.

Figure 17
Yount, Maiken, Baker

Pressure Graph:

Ascent Profile For Repetitive Dive Of Forward Dive Series 2B
Inert Gas Loadings Versus VPM Criterion for Bubble Formation

Shown Upon Surfacing: Lines of Fixed Gradient = Isopleths of Constant Bubble Number
Calculated Based on Minimum Initial Radius (microns) of Gas Nuclei at Start of Dive Series

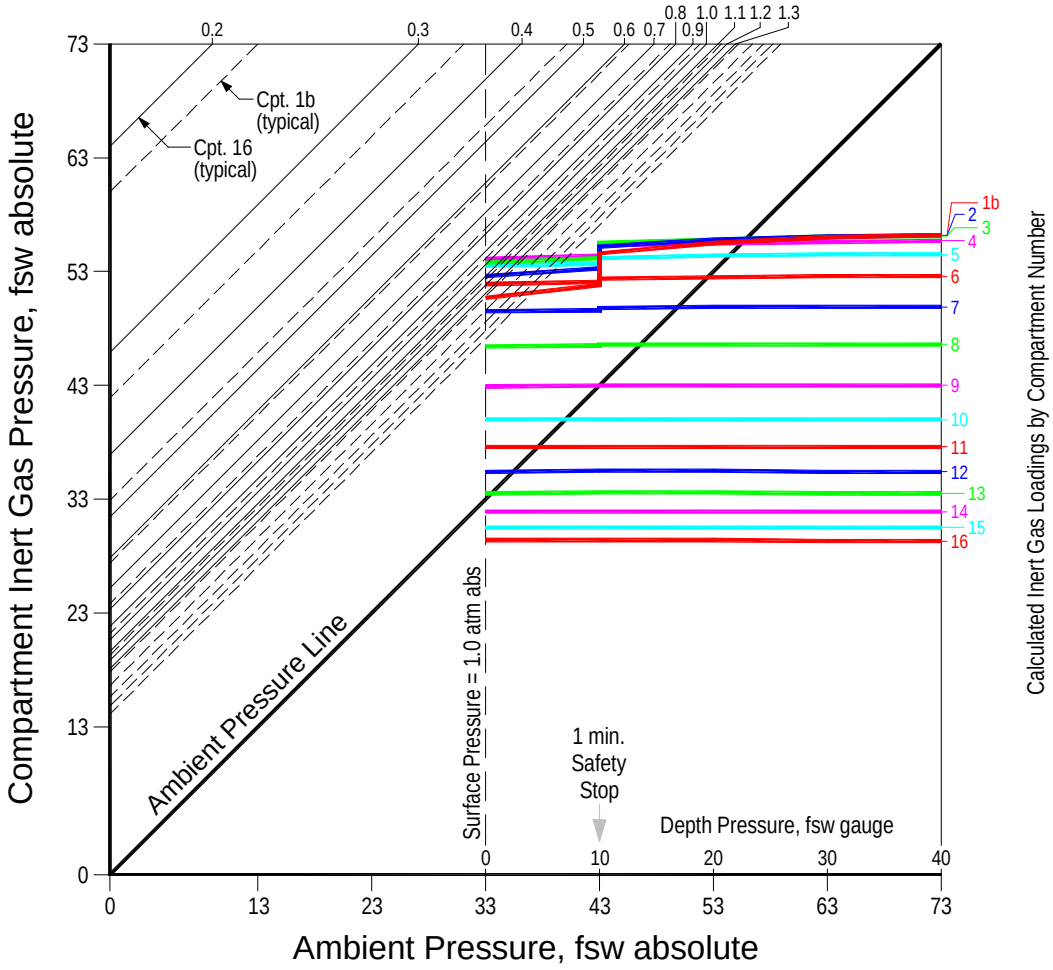

Notes:

1. After surface interval of 60 minutes, repetitive air dive to 40 fsw for 106 minutes bottom time (no-deco limit).
2. Inert gas is nitrogen. Gas loadings are shown leaving the bottom at the end of the bottom time.
3. Ascent rate is 30 fsw/min. Descent rate is 75 fsw/min and descent is included in the bottom time.
4. VPM criterion is computed with varying differential crushing and supersaturation pressures across the 16 compartments.

Observations:

1. Bubbles are formed in Compartments 1b thru 7 upon surfacing from this dive.
2. Overpressure (supersaturation) gradients will exist for over 30 minutes after this dive to drive bubble growth.
3. There is a difference of 4.0 fsw in allowable gradients between Compartments 1b and 16.

Figure 18
Yount, Maiken, Baker

Pressure Graph:

Ascent Profile For Repetitive Dive Of Forward Dive Series 3B
Inert Gas Loadings Versus Conventional M-values

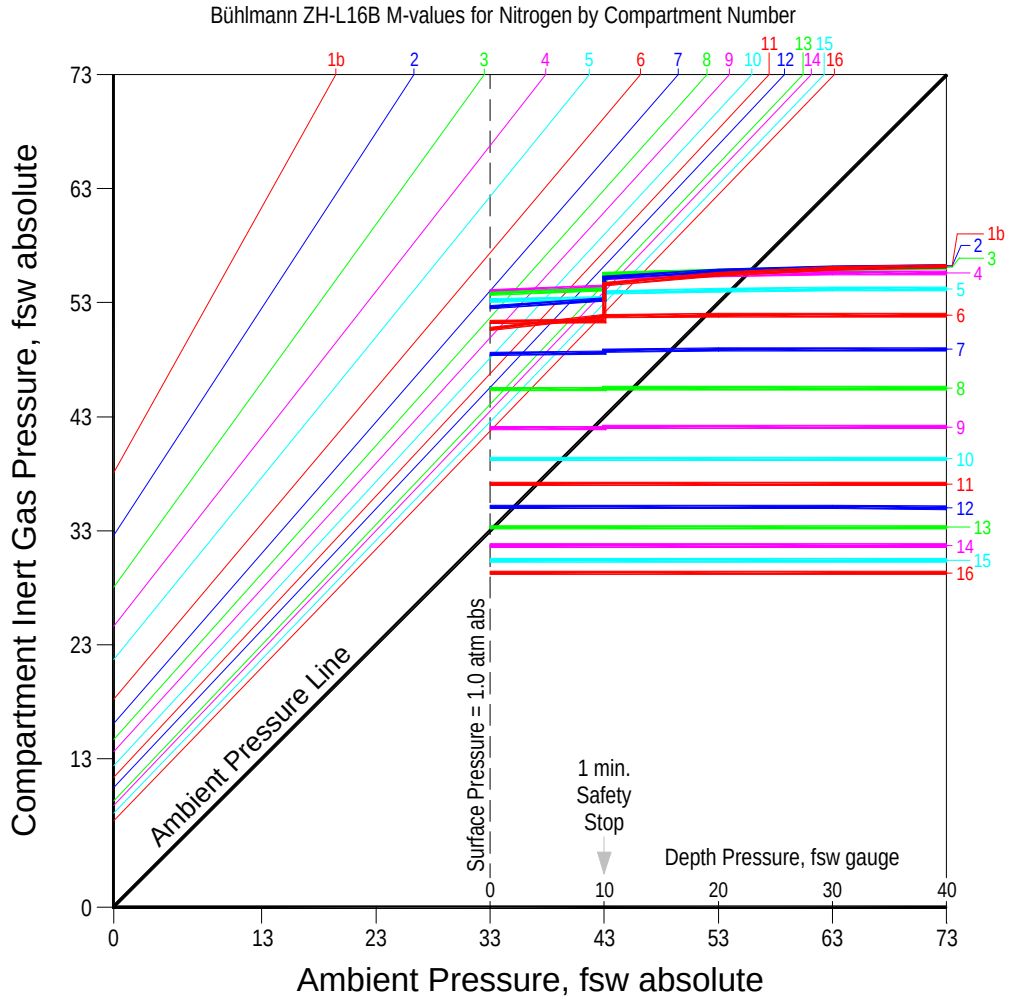

Notes:

1. After surface interval of 120 minutes, repetitive air dive to 40 fsw for 106 minutes bottom time according to no-deco limit of Bühlmann ZH-86 Air Diving Tables.
2. Inert gas is nitrogen. Gas loadings are shown leaving the bottom at the end of the bottom time.
3. Ascent rate is 30 fsw/min. Descent rate is 75 fsw/min and descent is included in the bottom time.
4. A one minute safety stop is required by the table.

Observations:

1. M-values for fast compartments permit large overpressure gradients and thus allow profuse bubble formation.
2. Upon surfacing from this dive, Compartments 6 and 7 are leading (gas loadings closest to M-values).
3. The one minute safety stop at 10 fsw has only a mild effect in terms of dropping gas loadings.

Figure 19
Yount, Maiken, Baker

Pressure Graph:

Ascent Profile For Repetitive Dive Of Forward Dive Series 3B

Inert Gas Loadings Versus VPM Criterion for Bubble Formation

Shown Upon Surfacing: Lines of Fixed Gradient = Isopleths of Constant Bubble Number
Calculated Based on Minimum Initial Radius (microns) of Gas Nuclei at Start of Dive Series

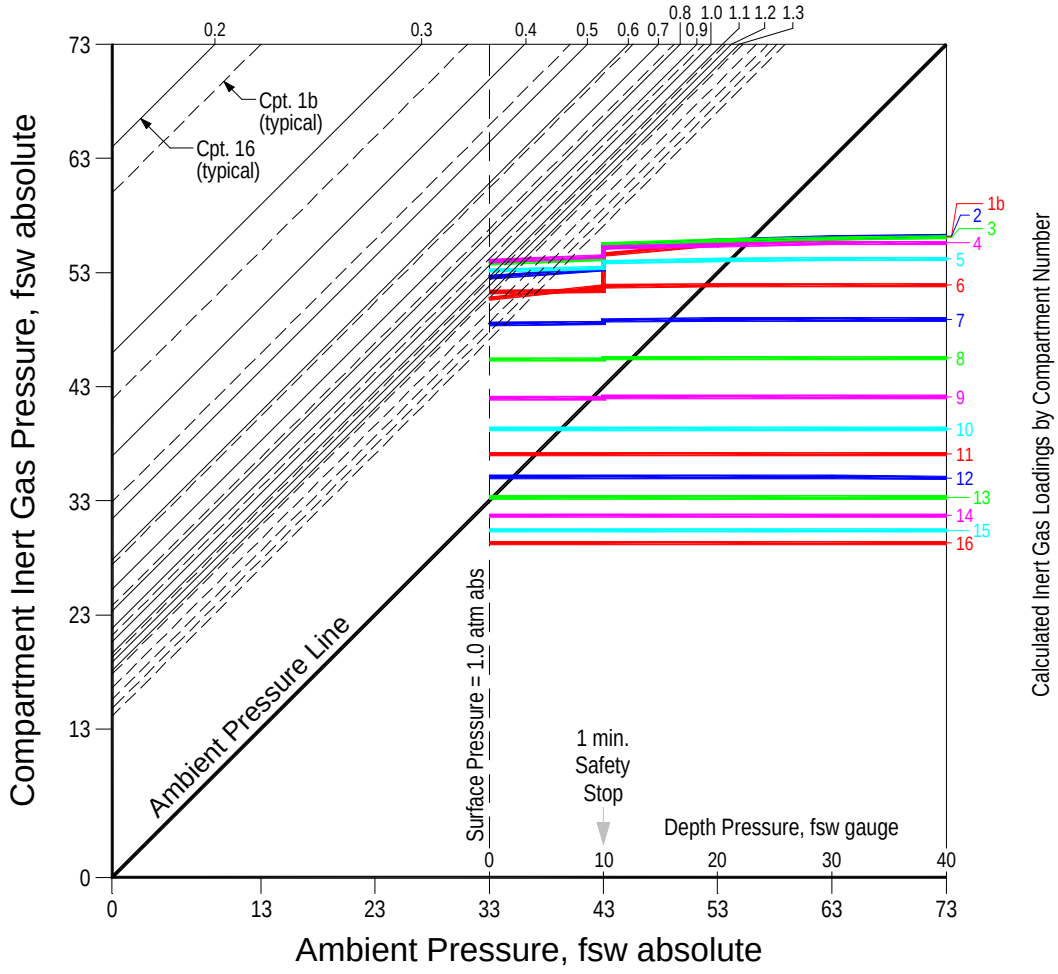

Notes:

1. After surface interval of 120 minutes, repetitive air dive to 40 fsw for 106 minutes bottom time (no-deco limit).
2. Inert gas is nitrogen. Gas loadings are shown leaving the bottom at the end of the bottom time.
3. Ascent rate is 30 fsw/min. Descent rate is 75 fsw/min and descent is included in the bottom time.
4. VPM criterion is computed with varying differential crushing and supersaturation pressures across the 16 compartments.

Observations:

1. Bubbles are formed in Compartments 1b thru 7 upon surfacing from this dive.
2. Overpressure (supersaturation) gradients will exist for over 30 minutes after this dive to drive bubble growth.
3. There is a difference of 4.0 fsw in allowable gradients between Compartments 1b and 16.

Figure 20
Yount, Maiken, Baker